ZAROMB RESEARCH

Energy Conversion, Electrochemical and Electro-Optical Projects

376 Monroe Street Passaic, New Jersey 07055 Area Code 201 778-1770

HYDROGEN-OXYGEN FUEL CELL SYSTEM WITH REACTANT-SUPERSATURATED ELECTROLYTE FEED

by

Solomon Zaromb

FINAL REPORT

July 10, 1967

for

NASA Headquarters
Washington, D. C. 20546

Contract NAS 7-531

HYDROGEN-OXYGEN FUEL CELL SYSTEM WITH REACTANT-SUPERSATURATED ELECTROLYTE FEED

by

Solomon Zaromb

FINAL REPORT

July 10, 1967

for

NASA Headquarters
Washington, D. C. 20546

Contract NAS 7-531

HYDROGEN-OXYGEN FUEL CELL SYSTEM WITH REACTANT-SUPERSATURATED ELECTROLYTE FEED

by

Solomon Zaromb

FINAL REPORT

November 21, 1966 to May 20, 1967

Prepared for:

Code RNW

National Aeronautics and Space Administration

Washington, D.C. 20546

Contract NAS 7-531

July 10, 1967

ZAROMB RESEARCH CORPORATION

376 Monroe Street

Passaic, New Jersey 07055

FOREWORD

This work, performed under Contract NAS7-531, was monitored by Mr. Ernst M. Cohn, Head, Electrochemical Systems, NASA Headquarters, Washington, D.C., whose stimulating and helpful suggestions and observations contributed significantly to the over-all results. Other NASA personnel who contributed through fruitful comments included Messrs. R. Boehme, N. H. Hagedorn, H. McBryar, and H. J. Schwartz. Mr. Milton C. Stone, Technical Coordinator, Ametek, Inc., Paoli, Pa., and Mr. Edwin F. Gregg, Professional Engineer, served as consultants on the fluidic control and valve system outlined in Section II-3. Acknowledgments are also due to Dr. H. M. Hershenson, Assistant Director, Advanced Materials Research and Development Laboratory, Pratt & Whitney Aircraft (PWA), North Haven, Conn., who kindly supplied excerpts from an internal PWA report by Dr. J. G. Tschinkel, and to Dr. Ingemar Lindholm of ASEA, Fuel Cell Research, Västerås, Sweden, who kindly forwarded an unpublished report by Dr. G. Eklund. These two reports have served to fill in the wide gaps in the published data on the solubilities of hydrogen and oxygen in alkaline electrolytes.

SUMMARY

A conceptual design analysis was performed for the purpose of evaluating the feasibility and advantages of a supersaturated feed fuel cell (SFFC) based on packing reactants into electrolyte solutions under high pressure followed by circulation of the loaded electrolytes through appropriate porous electrodes. This study was confined to low temperature alkaline H_2-O_2 fuel cells.

Tentatively assumed normal operating conditions of 75 ^{o}C at 10 atm system pressure and 200 atm reactant saturation pressures, 5 M KOH, and 0.25 amp/cm^2 apparent electrode area, yield a predicted output voltage of at least 1.10 v/cell for the SFFC as compared with only 0.90 v/cell or less for gaseous-diffusion type (GDT) or for recently considered undersaturated flooded-flow (UFF) systems. This voltage increase of more than 20% is obtained in spite of a rather high apparent current density because of:

a) a gain of 0.10-0.12 v in theoretical emf deriving from the free energy of expansion of pressurized gases (Nernst potential);

b) a reduction in cathodic activation polarization of at least 0.10 v deriving from:

1. increased exchange current density with increased reactant partial pressure;

2. higher available catalyst area obtainable with flooded-flow electrode structure; and

3. better accessibility and utilization of the available catalyst area; and

c) reduced anode concentration polarization and reduced ohmic losses within the electrode structures again resulting from the improved accessibility of catalytic sites.

Superior electrode performance may also be expected from accelerated product and heat removal from the active sites.

Reactant and product transport via the circulating electrolyte also increases the peak power capability to 4-6 times the rated power.

The voltage gain of more than 20% results in a corresponding increase in energy efficiency and hence in a proportionate decrease in reactant and storage tank weights. The improved energy efficiency also results in decreased heat generation and hence in a decrease of over 30% in required radiator weight. This saving together with the major reduction in fuel cell stack weight afforded by the increased power density results in a net saving of over 20% in total equipment weight. An over-all saving of at least 20-30% is thus obtained with the SFFC regardless of mission length.

Since the reactants and tanks constitute the predominant weight items in longer missions, even small percentage savings

in reactant consumption may be of importance. A 6-15% increase in energy conversion efficiency may then be effected by means of a thermal engine driven by the heat generated in the fuel cell reaction. Such an engine could amply take care of all the accessory pumping and pressurization power requirements which amount to less than 3% of the fuel cell output.

A higher operating temperature, e.g., 100-150 °C, should result in further reduction in polarization and ohmic losses and hence in further weight savings. However, additional solubility data will be required to ascertain the optimum temperature region.

Saturation pressures in excess of 200 atm, possibly as high as 600 atm, might also yield additional advantages. However, beyond 600 atm any marginal gains would probably be outweighed by increased pressurization and pumping power requirements and increased equipment weight.

The SFFC system is shown to be stable and in part self-regulating. It is also readily amenable to external control by either electronic or fluidic circuitry. In spite of the required additional components, the system as a whole appears to be simpler, more rugged, and more reliable than GDT systems, chiefly because of simplifications and functional improvements in the fuel cell stack

The negligible rate of electrode deterioration and the increased lifetime to be expected with the SFFC may be of special importance in long missions.

Further work should be aimed first of all at the experimental verification of the expected advantages of a small SFFC utilizing conventional accessory equipment. The design, construction, and testing of compact saturation chambers, pumps, and controls could thereafter lead to a perfected system.

CONTENTS

LIST OF FIGURES

OBJECTIVE

This report assesses the feasibility and advantages of high-performance flooded-flow H_2-O_2 fuel cells wherein the required mass and heat transport to and from active electrode sites would be effected through circulation of reactant-supersaturated electrolytes. Such circulating electrolytes may be expected not only to overcome the diffusion and heat transfer limitations encountered with gas-filled electrodes, but also to result in higher exchange current densities and open-circuit voltages, and consequently in higher over-all energy conversion efficiency and in reduced powerplant and reactant weights.

This study is confined to alkaline type fuel cells operating at low or moderate temperature.

I. BACKGROUND

I-1. Drawbacks of Gas-Diffusion Electrodes

The operation of present H_2-O_2 fuel cell electrodes is dependent on dissolution of gaseous reactants at gas-electrolyte interfaces within electrode pores followed by reactant diffusion through the electrolyte toward the active catalyst sites at the pore walls (1-7). However, the low solubilities and diffusivities of H_2 and

O_2 in aqueous electrolytes necessitate short diffusion paths in order for the mechanism to proceed at an appreciable rate. Most of the electrochemical activity must therefore be confined to thin meniscus films within the electrode pores. Moreover, the ionic conductance through the electrolyte along a thin meniscus film must be quite low and must decrease with the distance from the meniscus tip. Hence, the major electrochemical activity tends to be concentrated in fairly narrow meniscus regions which may extend to a depth of only around $10^{-5 \pm 1}$ cm (8, 9). Such concentration of electrochemical activity implies:

a) less than 1% utilization of the available catalyst area, the usual electrode thickness being in excess of 10^{-2} cm; and

b) a tendency towards local overheating in the active regions with concomitant deactivation of catalytic sites (8-10).

Such deactivation may in turn account for or contribute to the observed gradual deterioration of fuel cell electrodes after several hundred hours of continuous operation (11, 12).

I-2. Flow-Through Electrodes

It may be readily seen that the above difficulties could be avoided by filling the electrode pores with cir-

culating reactant-rich electrolyte. Besides providing increased heat absorption capacity, the circulating electrolyte would serve to carry the reactants to the catalytic sites and remove the reaction products from the electrode pores. The effective ionic conductance along the pore walls would also be increased considerably, since no non-conductive gas-filled spaces would be obstructing the current through the electrolyte. Neither would the pores have to be occluded by non-conductive wet-proofing agents. A much larger fraction of the available catalyst area can thus be allowed to participate in the fuel cell reactions.

Such a "flow-through" or "flooded-flow" H_2-O_2 fuel cell system was already thought of and tested by Bacon back in 1939 (13). Although Bacon's flow-through electrodes could yield current densities of up to 81 ma/cm^2 at 0.65 v/cell, they were abandoned as inferior to the gas-diffusion electrodes because of apparent transport rate limitations. The latter might be attributed to the low solubility of gases in KOH solutions under Bacon's operating conditions - 27% KOH solution at 240° C and 1,075 psi. According to data from several sources (14-20) plotted in Fig. 1, the solubility of H_2 and O_2 in 27% KOH solution decreases with increasing temperature at the rate of around 0.5%/° C in the range between 21° C and 75° C.

A similar trend is exhibited at higher temperatures for the solubility of H_2 in 75-82% KOH solutions between 170 °C and 200 °C (Fig. 1c). Hence, the solubility of H_2 and O_2 in 27% KOH at 240 °C should be at least an order of magnitude lower than at 75 °C, i.e., of the order of 10^{-5} M at 1 atm solute pressure. At Bacon's maximum pressure of around 75 atm the solubility might increase at most to circa 10^{-3} M, which would still require an electrolyte flow rate of at least 1 $cc\text{-}cm^{-2}\text{-}sec^{-1}$ or 15 $gal/min/ft^2$ for a current density of around 100 amp/ft^2. The relatively poor performance of Bacon's flow-through electrodes is therefore hardly surprising.

More recently Meissner and Reti (21, 22) experimented with a flow-through system at room temperature and atmospheric pressure. However, the low solubilities of H_2 and O_2 at low or moderate pressure would again require inordinate flow rates for high power operation.

I-3. Low-Temperature High-Pressure Flooded-Flow Fuel Cell

In a quite recent optimization analysis, Reti and Sadek (23) propose a flooded-flow system operating at 50 atm and room temperature (291 °K) to 373 °K. These conditions begin to approach those selected in the present study, but they still fall far short from the optimum arrived at below.

According to Fig. 1, the solubility of H_2 would

exceed 10^{-4} M in the ranges of less than 30% KOH at less than 75 °C or of more than 90% KOH at 170 °C to 200 °C. Moreover, the solubility of O_2 in 5 M KOH solutions obeys Henry's law up to a pressure of at least 10 atm (17, 24). Assuming Henry's law to be approximately valid up to 200 atm, one would expect at equilibrium around 0.03 M H_2 or O_2 in 5 M KOH solution at 75 °C and 200 atm solute pressure. Under these conditions, the reactant concentration would be at least 30 times higher than in Bacon's early experiments, which could yield at least 30-fold higher current densities, i.e., several amp/cm^2, at comparable electrolyte flow rates.

Higher reactant pressures would also yield a higher output voltage and hence a higher energy conversion efficiency, with considerable savings in the weights of reactants and storage tanks (cf. Sec. IV). These voltage and energy gains arise from:

a) increased open-circuit voltage (cf. Sec. I-6);

b) decreased diffusion polarization losses (cf. Sec III-4.e.i.); and

c) increased exchange current densities and hence reduced activation polarization (cf. Sec. III-4.e.ii.).

Electrolyte saturation at high reactant pressures may therefore yield superior flow-through electrodes provided that certain objectionable features of high-pressure

operation be satisfactorily circumvented.

I-4. Supersaturated Electrolyte System

To have an entire fuel cell system pressurized to more than 100 atm would hardly be practical, as a sizable pressure-resistant enclosure could easily outweigh the savings to be expected from improved fuel cell performance. However, it appears possible to operate most of the system at moderate pressure, e.g., at around 10 atm, and merely saturate the circulating electrolytes with the reactants in compact high-pressure chambers. Upon leaving a high-pressure chamber, the electrolyte would instantly become supersaturated, and gas bubbles would tend to form, but the rate of bubble formation could be kept down to a small percentage of the rate of reactant consumption at the flow-through electrodes (cf. Sec. III-5). The latter would then yield the enhanced performance to be derived from increased reactant concentration, just as in a highly pressurized system, in spite of being maintained at a merely moderate pressure.

The possibility of utilizing gas-supersaturated electrolyte in flow-through fuel cell electrodes is the key point of this study.

I-5. Stability Condition

The rapid release of pressure from the fluid leaving

the saturation chamber does not introduce any explosion hazard, because the concentration of dissolved gases must still remain rather small. The solubilities of H_2 and O_2 in 5 M KOH solution being less than 2×10^{-4} M at 1 atm pressure (cf. Fig. 1), even pressurization to 200 atm could not raise this concentration much above 3×10^{-5} mole/cc. Now, 3×10^{-5} gm-mole of gas at 75 °C and 10 atm would occupy a volume of less than 0.1 cc. Hence, even complete degassing of the supersaturated electrolyte could not increase the total volume by more than 10%. It should therefore be necessary and sufficient to provide room for a 10% volume expansion within the electrolyte circulation system, e.g., by using expandible tubing or containers, to preclude any excess pressure build-up.

I-6. Thermodynamic Aspects

According to the well-known Nernst relation, the reversible voltage E_{rev} of an H_2-O_2 fuel cell should increase with the respective partial pressures p_{H_2} and p_{O_2} at the electrode surfaces

$$E_{rev} = E^o + (RT/F) \ln (p_{O_2}^{\frac{1}{4}} p_{H_2}^{\frac{1}{2}})$$

where E^o is the reversible potential at unit reactant pressures (1 atm), R is the gas constant, T is the absolute temperature, and F is a Faraday. For a 5 M KOH

solution at 75 °C and $p_{O_2} = p_{H_2} = 100$ atm, the second right-hand term of Eq. (1) amounts to approximately 0.10 v, as compared to the E^o value of 1.19 v (25). For $p_{O_2} = p_{H_2} = 200$ atm, this second term amounts to 0.12 v.

In a supersaturated electrolyte, the values of p_{O_2} and p_{H_2} would tend to approach the ambient pressure asymptotically with time, but their instantaneous values upon leaving the saturation chambers would not decrease appreciably as long as the gases remain mostly dissolved in the electrolyte, since the partial pressure of a solute is approximately proportional to its concentration in accordance with Henry's law. One may therefore expect an open-circuit voltage gain of 0.10 to 0.12 v for saturation pressures of around 200 atm.

This gain in voltage and hence in over-all energy conversion efficiency derives simply from the utilization of the free energy of expansion stored in any high-pressure or cryogenic gas supply. In present fuel cell systems this expansion energy is wasted in the pressure-reducing valve.

In inactive gas-supersaturated electrolytes this expansion energy would also tend to be wasted in spontaneous bubble formation. However, circulation of the supersaturated electrolytes through active electrode

pores would channel this available free energy of expansion into useful electrical work.

Also wasted in present systems is the thermal energy dissipated in the fuel cell reaction. Even in a perfectly reversible cell the difference between the free energy and the enthalpy of water formation would be equivalent to around 0.25 F-v/F = 0.25 v. In cells operating at rated load, the ohmic and polarization losses are likely to amount to an additional 0.17 v even with the highly efficient system to be described in Sec. II and III. Total heat generation would then amount to around 0.42 v/1.15 v $\simeq$ 36% of the net power output. This heat, generated at a fuel cell temperature of around 350 ^{o}K, would be absorbed by surroundings having an effective temperature of less than 290 ^{o}K (26) and possibly even as low as 200 ^{o}K (27). Since a reversible heat engine operating between 200 ^{o}K and 350 ^{o}K could convert around 43% of the absorbed heat into useful work, it should be possible, in principle, to obtain additional power possibly approaching as much as 43% x 36% $\simeq$ 15% of the fuel cell output.

Even a 15% efficiency gain might usually not warrant the additional weight and complexity of a heat engine system. However, when most of the elements of a heat engine are already present or required anyhow, they might

just as well be made to yield maximum energy efficiency without substantially complicating or weighting down the over-all system. In particular, it may be noted that:

a) efficient heat exchangers are required anyway to remove the heat generated in the fuel cell; and

b) a boiling or condensing liquid provides a most efficient heat exchange fluid (28).

Furthermore, a boiling liquid can also yield pressurized vapor capable of driving a turbine, piston, or motor which could in turn drive the pumps and/or compressors required in the electrolyte-circulation and saturation system described in Sec. II. The energy available from the dissipated heat could thus provide not only all the required pumping power, but even some excess power to supplement the electrochemical fuel cell output, as shown in Sec. II-2.c.

II. SYSTEM REQUIREMENTS

The rather simple approach outlined in Sec. I does not seem to call for any undue complexity. Indeed, a detailed comparison with existing complete fuel cell systems reveals significant simplifications and increased reliability resulting from the supersaturated electrolyte feed. These gains will be found to arise chiefly from major improvements in the fuel cell stack and from the redistribution of essential functions among a larger number of simpler components, each of which is especially suited for its required task. The Chief flaws of gas-diffusion electrodes, as outlined in Sec. I-1, may be related to those functions for which these electrodes are not inherently suited. Once relieved of such unnecessary burdens, the fuel cell stack is enabled to develop more fully its electrochemical potential.

II-1. Electrolyte Supersaturation and Circulation System

The essential and also some optional components of an operable supersaturation and circulation system are indicated in Fig. 2. Starting from the right-hand side of the flow-diagram, cryogenic H_2 stored at around 10 atm is fed into a well-insulated chamber, wherein

it is compressed to around 200 atm and injected at high speed at appropriate intervals into an electrolyte-saturation chamber through a multiple-outlet atomizing nozzle.

In order to minimize the pumping power requirements, the liquid hydrogen injection step must be timed in accordance with the following cycle:

1. With valves B and C open and valve A closed, reactant-deficient electrolyte is allowed to fill the absorption chamber at the moderate system pressure of around 10 atm. No significant pressure differential across valves B and C is required in this step.
2. Valves B and C are first fully closed and then valve A is quickly opened for a brief time interval (1-10 msec) so as to allow rapid injection of a metered volume of liquid H_2. The high pressure

differential across valve A -- circa 200 atm -- should be adequate to ensure atomization and dispersal of fine liquid H_2 droplets throughout the absorption chamber.

3. With valves A, B, and C closed, the fluid confined in the absorption chamber is pressurized through rapid vaporization of the liquid H_2 and is further compressed hydraulically to a pressure of around 200 atm. Saturation of the electrolyte should be accelerated by the pressure waves generated in steps 2 and 3 and by the instability of fine liquid H_2 droplets dispersed in warm electrolyte.

Following step 3, the saturated electrolyte is displaced by partly depleted electrolyte as outlined in step 1. After passing through a hydrogen-activity sensor (see p.27), the enriched electrolyte is distributed among multiple inlet lines and forced by a multi-channel pump into the separate H_2-electrode compartments of the fuel-cell stack.

The multi-channel pump may be of the peristaltic type or of any other variety which could be easily driven by a single shaft and which would tend to break any electrical leakage paths through the electrolyte between series-connected cells. In order to prevent such leakage paths, the H_2-rich electrolyte leaving the fuel cell stack

should pass through a similar multi-channel pump. At the exit from the latter pump the channels may be combined into a single line passing through a hydrogen activity sensor, water and heat removal system, and a gas-liquid separating or gas-dispersing filter leading back to the saturation chamber.

The left-hand side of Fig. 2 outlines an essentially similar saturation and circulation scheme for the O_2-enriched electrolyte. However, the water and heat removal system may be dispensed with on this side, as the water forms on the hydrogen side in alkaline fuel cells, and heat conduction within the fuel cell stack would prevent excessive temperature gradients between the O_2 and H_2 electrodes. Any moderate temperature gradient could even have the beneficial effect of increasing the exchange current density and hence reducing the polarization at the oxygen electrode (cf. Sec. III-4.d.).

II-2. Essential Components

a. Saturation Chambers

Each saturation chamber (Fig. 3) is connected directly to three valves, and is also acted upon by a piston acting on a hydraulic oil acting on a diaphragm. In missions of long duration, the piston power may be proveded by a thermal engine, as proposed in Sec. I-6. The maximum volume displacement

of the piston and diaphragm may amount to only around 0.1 to 1 cc (cf. Sec. III-3.c.). Both the piston and the diaphragm can therefore be fairly rugged and compact.

Around 100 or 200 cc/sec of electrolyte would have to be circulated through each saturation chamber per 1 kw power output. Thus, in a system designed for cycling rates of between 0.5 and 10 cps and a power output range of between 0.5 and 10 kw, around 100 or 200 cc electrolyte would have to be saturated in each cycle. This would require a saturation chamber capacity of around 100 or 200 cc for a 2-kw powerplant capable of yielding a peak power of 10 kw, i.e., operating at the rate of 1 cps per kw power output.

The weight of a 100- or 200-cc saturation chamber capable of withstanding around 200 atm pressure can be readily estimated from the weights of currently available high-pressure containers. Thus, a 150-ml Monel double-connection type sampling cylinder rated for a maximum operating pressure of 5,000 psi (Hoke No. 4 HDM 150) weighs only $1\frac{1}{2}$ lb (29). Hence, a 3,000-psi pressure chamber would require a cylinder weight of around 2 lb with conventional alloys. With the stronger alloys developed in recent years, such as the low-carbon chrome-molybdenum steel used for low-weight high-pressure gas tanks, the required cylinder weight would come closer

to $\frac{1}{2}$ lb/100 cc capacity (30). However, in view of the somewhat more complex geometry of the saturation chamber of Fig. 3, a weight of 1 lb/100 cc capacity will be assumed in the estimates of Sec. IV-1.

In order to effect rapid and nearly homogeneous dissolution of the injected gas throughout the electrolyte volume, a multiple nozzle arrangement is required such as that shown in Fig. 4. These multiple nozzles should be distributed uniformly over at least one complete side of the saturation chamber, as shown in Fig. 3. Once the nozzles are properly distributed so as to inject a mist of liquid H_2 or O_2 droplets uniformly dispersed throughout the chamber, it can be easily shown that the equilibration time need not exceed 10^{-3} to 10^{-2} seconds. The volume ratio of electrolyte to liquefied reactant being of the order of 100 cc/0.1 cc $\simeq 10^3$, the particles contained in each droplet would have to diffuse to an average maximum distance

$$\overline{d_m} \simeq 10\bar{r} \qquad (2),$$

where $\bar{r}$ is the average droplet radius. Moreover, the rms displacement $(\overline{d^2})^{\frac{1}{2}}$ of a particle by diffusion within a time t_d is given by (31)

$$\overline{d^2} \simeq 2Dt_d \qquad (3),$$

where D is the diffusion coefficient of a given particle species within a given medium. Equilibration might be considered as nearly complete for

$$(\overline{d^2})^{\frac{1}{2}} \simeq \bar{d}_m \qquad (4),$$

as the average particle would by then have diffused through the maximum required distance. Eqs (2) through (4) thus yield an equilibration time

$$t_{eq} \simeq (10\bar{r})^2/2D \qquad (5).$$

Thus, for $D \simeq 10^{-5}$ cm^2-sec^{-1} and $\bar{r} \simeq 10^{-4}$ cm, $t_{eq} \simeq 0.005$ sec. Sufficiently rapid equilibration should therefore be achievable with nozzles yielding an average droplet radius of 1 micron.

The above rapid homogenization and saturation approach may be akin to that utilized in several widely used rapid ultrasonic emulsifiers which also act via injection of liquids through nozzles at high pressures (32). Moreover, the present homogenization process is greatly facilitated by the instability of liquid H_2 or O_2 droplets in hot aqueous solutions. This instability should counteract or eliminate the usual interfacial barriers to the mixing of different fluid phases.

b. Fuel Cell Stack

i. Electrode Configuration. The electrode configuration

in a single cell is shown schematically in Fig. 5. The anodic and cathodic electrolyte streams are separated by a microporous hydrophilic matrix which permits ion transport by conduction but impedes convective mixing of the streams. In order to minimize such mixing, the micropores within the separator matrix should be at least an order of magnitude smaller than those in the porous electrodes, i.e., around 0.1 micron or less. Moreover, in order to distribute the flow about uniformly through the electrode pores and yet avoid excessive pressure drops, narrow baffled channels are provided at the back and front of each electrode.

For minimum pumping requirements only three baffles are required per electrode -- two placed near the ends on one side of each electrode and one placed midways on the opposite side. The electrolyte is then forced to flow nearly perpendicularly to the face of each electrode, entering from the back of the electrode on one side of the central baffle and then re-entering frontally through the other half of the apparent electrode area. The electrolyte must thus pass through two electrode thicknesses.

The channel or gap widths L_g between the inner electrode surfaces and the separator matrix or between the back surfaces and the outer cell walls need not exceed

0.01 cm, which is ample to permit nearly free flow alongside the electrode surfaces, the mean pore diameter within the electrodes being around 100 times smaller (10^{-4} cm). In order to maintain L_g constant over the entire active area, the electrodes must be covered on both sides by multiple 0.01 cm thick discs of sufficiently small diameter to constitute no obstruction to electrolyte flow. The discs attached to the inward surfaces may be non-conductive, so as to prevent any electrical shorting through flaws in the separator matrix , whereas the outer discs may be metallic so as to provide electrical contact to current collectors at the cell walls.

The cell wall may consist of a single solid nickel sheet around 0.02 cm thick, shared with and providing electrical contact to an adjacent cell in a bipolar electrode type of series-connection, in which case the wall thickness attributable to a single cell would be only $L_{ws} \simeq 0.01$ cm. Alternately, the metallic current-collecting sheet may have to be insulated from the next cell in order to allow a parallel cell connection, in which case the single cell wall thickness would have to be at least $L_{wp} \simeq 0.02$ cm.

Thus, with a cathode thickness $L_c \simeq 0.01$ cm, anode thickness $L_a \simeq 0.0025$ cm, separator thickness $L_s \simeq 0.04$ cm, and alternating parallel and series connections between

adjacent cells, the total cell thickness L_T becomes

$$L_T = L_{wp} + L_{ws} + 4L_g + L_a + L_c + L_s \simeq 0.123 \text{ cm}$$

Thus, with pairs of cells connected in parallel, a 30-pair fuel cell stack would have a total thickness of

$$30 \times 2 \times 0.123 \text{ cm} \simeq 7.4 \text{ cm},$$

excluding the end plates.

ii. Prevention of electrical leakage paths through the electrolyte. To minimize leakage currents through the electrolyte between series-connected cells one may either resort to special manifolding, as has been practiced with one type of Zn-air battery (33) and as was also proposed by Reti and Sadek (23). This approach may have the advantage of simplifying the pumping system and the electrolyte connections to the cell stack. However, even small leakage currents at voltage differences of more than 3 v may cause slow electrode deterioration through deplating of metal from some electrodes and dendritic growth on others. It may therefore be preferable to separate the electrolyte lines by resorting to a multichannel pump, as proposed earlier (cf. Sec II-1 and Fig. 2).

A 35-volt stack (comprising 30 cell-pairs at 1.15 volt/cell) would then require 60 inlets and 60 outlets,

half for the H_2-rich and half for the O_2-rich electrolytes. To avoid crowding of channels, the baffles on the anodes and cathodes should not be parallel to each other, as suggested in the schematic drawing of Fig. 5, but should rather form two perpendicular sets. The anodic electrolyte flow across each cell could thus proceed from left to right, while the cathodic flow proceeds from top to bottom (or the other way around). The appropriate inlet and outlet channels could then be arranged approximately alongside (but not along the full length of) the respective baffles. With each inlet feeding one cell-pair around 0.25 cm thick, and with the inlets and outlets disposed partway along 4 cell sides, excessive crowding of channels is easily avoided.

iii. Size and weight of fuel cell stack. As shown in Sec. III-4, the active fuel cell volume and weight need not exceed 450 cm^3/kw and 2.7 lb/kw, respectively. However, when provision is made for edges, gaskets, and end plates, these values may double. Thus, a 5-kw fuel cell stack would have a total volume of around 4,500 cm^3 (e.g., 10 cm x 18 cm x 25 cm) and a total weight of around 27 lb.

c. Water and Heat Removal System

As found in Sec. I-6, the rate of heat generation

would amount to around 36% of the fuel cell power even at 1.15 v/cell. At 1.10 v/cell the heat production would amount to 0.47 v/1.10 v $\simeq$ 43% of power output. In addition, water would be produced at the rate of

$$\frac{9 \text{ gm} \times 10^3 \text{ v-coul/sec/kw}}{1.1 \text{ v} \times 96{,}500 \text{ coul}} \simeq 0.085 \text{ gm-sec}^{-1}\text{-kw}^{-1}.$$

The latent heat of vaporization of water being 540 cal/gm, around 46 cal/sec $\simeq$ 190 watts must be carried away by water vapor transpiring through semi-permeable membranes. The remaining heat, amounting to (430-190) w/kw, is to be removed by a heat exchanger.

Since the rate of H_2-rich electrolyte flow is around 200 cm^3/sec/kw (cf. Sec. III-3.c.i.), the temperature rise within the electrolyte leaving the anodes would amount to only around $\frac{1}{2}$ °C. The difference between counter-current and other types of heat exchangers may therefore be negligible. Nevertheless, to maintain a proper water balance it appears preferable to bring the heat exchange fluid up to around 65 °-70 °C, in a counter-current arrangement and then allow the water to condense on the heat exchanger walls at around 68 °C, so as to obtain an approximate water vapor pressure equilibrium with the 5 M KOH electrolyte at 75 °C. This water removal and electrolyte composition control method is modelled after

the well known "osmotic still" (34).

To provide efficient heat transfer as well as thermal engine power the heat exchange fluid should be in the form of vapor-liquid mixtures at both its warm and cold ends. A suitable Freon composition should be usable for these requirements. On the warm side, at around 67 °C or 340 °K, the heat absorbed from the electrolyte and condensing water results in vaporization and pressure build-up in the Freon mixture. Expansion of the compressed vapor through a piston or turbine then yields thermal engine power and also effects partial cooling of the vapor, e.g., to around 290 °K. The cool low-pressure vapor condenses in a radiator facing the dark side of the sky, and the cool condensate is pumped back to the warm heat exchanger.

This entire operation represents the reverse of a standard refrigeration cycle (35). The theoretical engine efficiency under these conditions should be around 50 °K/340 °K $\simeq$ 14%. The engine could thus deliver a maximum of 0.14 x 430 w/kw $\simeq$ 60 w/kw.

Since the total parasitic power requirements should amount to less than 30 w/kw (cf. Sec. III-3), some excess heat engine power may be available for the performance of extra tasks, e.g., to compress the boil-off from cryogenic storage tanks or to produce saturation chamber pressures exceeding 200 atm.

II-3. Accessory Components

Many variants of the pumping and pressurization system, control system, and other accessories not already discussed appear to be feasible and perhaps equally acceptable depending on specific mission requirements. The following examples must therefore be regarded as merely suggestive or illustrative of some of the many options available to proficient designers.

a. Pumps and Pressurizing Devices

With the wide variety of available pumps, compressors, and pressure boosters (36, 37) there is plenty of room for flexibility in system design. Although several pumps are indicated in Fig. 2, only one or two custom-built units could take care of all the requirements. E.g., the medium-pressure pump(s) required for electrolyte circulation could also effect the compression of the cryogenic reactants and of the saturation chambers via such hydraulic pressure-boosting devices as a ram-and-piston or multiple diaphragm (37). Such an approach would also permit smoother continuous operation, as pumping of the electrolyte could then be allowed to proceed by diversion of the electrolyte into the pressure booster(s) during those time intervals when the saturation chamber is closed off.

Although a peristaltic type of multi channel pump was suggested earlier (Secs. II-1 and II-2.b.ii.) as a means of preventing leakage currents through the electrolyte, the same purpose could be achieved with a specially designed rotary pump having a compartmentalized impeller and multiple inlets or outlets facing different compartments. E.g., a regenerative pump with a turbine resembling a honeycomb, and close clearances between the impeller and the casing, as described and illustrated in ref. 36 (pp. 218-9, Fig. 6-24), may be ideally suited for this purpose.

It might also prove possible to adapt a radial piston type of pump. Such pumps are highly attractive in terms of performance capabilities, ruggedness, and compactness. E.g., a ball-shaped piston type described in ref. 37 (pp. 37-8 and 62) has a power to weight ratio of 2 hp/lb and performs equally well as a variable-speed motor and as a high-capacity pump.

b. Start-Up and Control System

i. Start-up. The priming required to supply reactants to the fuel cell stack could be effected electrically, hydraulically, or via an electronic or fluidic signal actuating an electric or hydraulic motor. If the continuous pumping power is to derive from the thermal

engine, as suggested in Secs. I-6 and II-2c., then a hydraulic motor driven directly by the thermal engine would seem superior to an electrical one. Such a motor could be initially driven by expansion of gaseous reactants drawn from the storage tanks. There may thus be no need for any auxiliary electrical power supply even at start-up. A simple fluidic circuit maintained by reactant boil-off could actuate a priming valve initiating gaseous flow through the hydraulic motor. Once the fuel cell stack has been supplied with reactants and has reached its proper operating temperature, a voltage signal can actuate a diverting valve to bring the thermal engine into action.

Alternately, when an auxiliary electric power source is available anyhow, conventional electrical start-up might be preferable. Since the maximum parasitic power requirements at full load would be less than 3% of output power (cf. Sec. III-3), a 10- to 30-watt power source should be adequate for priming purposes.

ii. Built-in versus external servo-controls. The thermal engine may provide a built-in servo-control, since the heat generated will be roughly proportional to the power output and will increase with increasing polarization, and an increase in the rate of reactant supply in proportion with the available thermal power would tend to reduce

polarization and thereby moderate the heat generation. However, such a control method may be too sluggish for some requirements. A positive computer-logic type of control mechanism may therefore be preferable. Nevertheless, the inherent servo-control feature associated with a thermal engine might make the latter attractive from the reliability viewpoint.

The external control signals may derive from a fuel cell voltage sensor, from reactant activity sensors, or from both, depending on the redundance required to ensure adequate reliability. The reactant activity sensors may consist simply of miniaturized fuel cells with small-area anodes facing larger cathodes or vice versa, with the current density and/or degree of polarization at the smaller electrode providing a measure of the reactant concentration in the tested electrolyte.

iii. Control System. Flow proportioning, sequencing, and adjustment to variable loads can be accomplished using fluidic or electronic control.

Since the optimum reactant feeding rate would be approximately proportional to the power output, the saturation cycle frequency should be varied accordingly. Such frequency control can be effected by a primary fluidic device system utilizing a brushless motor driven

by a variable frequency oscillator. The appropriate control signal, which may derive from a fuel cell voltage sensor and/or from the reactant activity sensors adjusts the oscillator frequency. The brushless motor rotates a vane which interrupts or establishes a fluidic path to or in opposition to an operation.

The fluidic switching logic is quite simple. Looking at the anodic loop (Fig. 2), one may start with valves B and C open. The H_2 activity sensor tests whether enough H_2 is fed to the fuel cell stack. As long as the H_2 activity on the inlet side of the stack remains high, valves B and C stay open. When the H_2 activity in the liquid leaving valve C falls below a pre-set value, valves B and C are closed. A delay ensues and A opens, squirts a metered volume of liquid H_2 into the saturation chamber, and then closes immediately. After a further delay the pressurizing piston D is allowed to proceed in the forward (compressive) stroke. After another delay, valves B and C are opened, piston D is reverted, and the cycle is repeated.

The above approach is only one of many possible ways of providing adequate reactant feed control.

c. Gas-Separating or Dispersing Filter

As shown in Sec. III-5, the rate of degassing of

the supersaturated electrolyte can be made negligible in comparison with the rate of reactant consumption by use of clean and fully wetted lyophilic materials within the entire electrolyte circulation system. The relatively small amount of gas evolved in a normal operating cycle could therefore be recompressed and redissolved in the electrolyte during the pressurization step. However, in order to effect more complete redissolution, the gas should be preferably broken up into microscopic bubbles. This could be effected by a gas-dispersing filter placed near the entry to the saturation chamber.

Alternately, the gas may be allowed to transpire through selectively permeable membranes and be fed to an auxiliary gas-diffusion type of fuel cell.

Gas-separation or venting means may also have to be provided at the inlets to each fuel cell electrode to prevent clogging by evolved gas. Alternately, each electrode may include highly gas-permeable areas (preferably adjacent to each of the baffles) through which any trapped gas would be automatically purged with continued electrolyte circulation.

III. DESIGN CALCULATIONS

III-1. Electrolyte Property Data and Choice of Composition and Operating Temperature

a. Solubilities of H_2 and O_2

The solubilities of H_2 and O_2 at 1 atm pressure and various temperatures are shown in Fig. 1 as functions of KOH concentration. The solubility of H_2 decreases with KOH content up to around 50 weight-% KOH and increases again in the range of 70-100% KOH. The solubility of O_2 follows a similar trend, at least up to around 50% KOH.

For concentrations of up to 30% KOH, the decrease in solubility corresponding to a temperature increase from 25 °C to 75 °C amounts to less than 20% for hydrogen and less than 40% for oxygen. For 5 M (23 wt-%) KOH, this decrease may amount to less than 15% for both gases. At 75 °C the solubilities of H_2 and O_2 in 5 M KOH are about 1.7×10^{-4} M and 1.8×10^{-4} M, respectively.

With increasing pressure the solubility appears to follow Henry's law, at least in the case of O_2 in 5 M KOH at 25 °C and 2-10 atm (17, 24).

b. Electrical Conductivity

At 18 °C, the electrical conductivity of KOH solutions reaches a maximum value of about 0.54 ohm^{-1}-cm^{-1} at around 25% KOH (38). This maximum conductivity should increase with temperature roughly in inverse proportion to the viscosity of water (39). One would therefore expect the conductivity of 5 M KOH at 75 °C to be around 1.5 ohm^{-1}-cm^{-1}. However, the measured value is closer to 1.1 ohm^{-1}-cm^{-1} (40).

c. Diffusivities of H_2 and O_2

The respective diffusion coefficients of H_2 and O_2 in 5 M KOH are approximately $D_{H_2} \simeq 1.4 \times 10^{-5}$ cm^2/sec at 30 °C (19) and $D_{O_2} \simeq 0.86 \times 10^{-5}$ cm^2/sec at 25 °C (16). Again assuming roughly inverse proportionality of solute mobility to solvent viscosity (39), one obtains for 75 °C in 5 M KOH $D_{H_2} \simeq 3.1 \times 10^{-5}$ cm^2/sec and $D_{O_2} \simeq 2.1 \times 10^{-5}$ cm^2/sec.

d. Compressibility of 5 M KOH Solution

The compressibilities β of aqueous electrolytes are given by the relation

$$\beta = \beta_o + Ac + Bc^{3/2} \qquad (6),$$

where β_o is the compressibility of pure water, c is the molarity, and the constants A and B have the following values for several electrolytes at 25 °C and 1 atm (41):

Electrolyte	A x 10^6	B x 10^6
LiCl	-4.97	0.84
NaCl	-5.91	1.04
KCl	-5.73	1.13
LiOH	-7.52	1.56
NaOH	-8.59	1.90

From the differential contributions of K^+ and OH^- ions one can estimate the values $A \simeq -8.4 \times 10^{-6}$ and $B \simeq 2.0 \times 10^{-6}$ for KOH. Furthermore, $\beta_o \simeq 45 \times 10^{-6}$ at 25 °C and 1 atm. Hence, the compressibility of a 5 M KOH solution at 25 °C and 1 atm should be approximately 25 atm^{-1}.

The value of β_o at 75 °C and around 100 atm is approximately the same as at 25 °C and 1 atm (38). Hence, the value $\beta \simeq 25 \times 10^{-6}$ atm^{-1} will be assumed to remain also valid under these conditions.

e. Choice of Electrolyte Composition and Temperature

In view of the relatively small decrease in reactant solubility with increasing temperature between

room temperature and 75 °C, the latter temperature has been tentatively selected for fuel cell operation. A higher temperature, e.g., 100 °C or even higher, might prove to be preferable when additional property data are obtained for the temperature range above 75 °C.

In view of the power density limit imposed by the ohmic losses through the electrolyte (cf. Sec. III-4), the optimum composition appears to be near the resistivity minimum, i.e., 5 M (or 23%) KOH.

III-2. Reactant Property Data and Choice of Pressure Conditions

a. Specific Volumes of H_2 and O_2

The densities of liquid H_2 and O_2 near their boiling points (-253 °C and -183 °C) are 0.071 gm/cc and 1.14 gm/cc, respectively (38). The corresponding specific volumes are therefore 14.1 cc/gm or 28.2 cc/mole H_2 and 0.88 cc/gm or 28.0 cc/mole O_2.

At 75 °C and 200 atm the available compressibility data (ref. 35, pp. 488-495) yield specific volumes of 158 cc/mole H_2 and 141 cc/mole O_2.

b. Choice of Operating Pressures

A maximum pressure of 200 atm in each saturation

chamber has been tentatively selected as an acceptable compromise value yielding enhanced fuel cell performance and efficiency without undue penalty in terms of parasitic power and/or equipment weight requirements.

A moderate pressure of around 10 atm has been tentatively selected for the remainder of the electrolyte circulation system.

III-3. Compressor and Pumping Power Requirements

a. Rate of Reactant Consumption

At an average output of 1 kw at 1.1 v/cell (cf. Sec. III-4.d.iv.) the rate of reactant consumption becomes

$$\frac{10^3 \text{ coul-v-sec}^{-1} \times 1 \text{ F}}{1.1 \text{ volt} \times 96{,}500 \text{ coul}} \simeq 9.4 \times 10^{-3} \text{ F/sec},$$

i.e., 4.7×10^{-3} mole H_2/sec plus 2.4×10^{-3} mole O_2/sec per kw power output.

b. Cryogenic Pumping Power

The power required for liquid reactant pumping is given by $\Delta P \Delta V/\Delta t$, where $\Delta P \simeq 200$ atm and $\Delta V/\Delta t$ is around 28 cc-mole^{-1} x 4.7×10^{-3} mole H_2/sec $\simeq$ 0.13 cc H_2/sec plus around 0.07 cc O_2/sec per kw power

output. Hence, the total cryogenic pumping power becomes approximately 200 atm x (0.13 + 0.07) cc-sec^{-1} $\simeq$ 4 w, i.e., around 0.4% of the power output.

c. Pressurization Chamber Power

i. Rate of electrolyte circulation. The respective solubilities of H_2 and O_2 in 5 M KOH being about 1.7 x 10^{-4} M and 1.8 x 10^{-4} M at 75 ^{o}C and 1 atm pressure, the corresponding values at 200 atm should be around 0.034 M and 0.036 M, according to Henry's law. Hence, the minimum required circulation rate must be around

$$\frac{4.7 \times 10^{-3} \text{ mole } H_2\text{-sec}^{-1}}{0.034 \text{ mole } H_2\text{-liter}^{-1}} \simeq 0.138 \text{ liter/sec}$$

per kw power output. However, to ensure minimum diffusion polarization the amount of H_2 transported should be around 50% higher than the amount consumed, i.e., at least 200 cc/sec/kw.

Similarly, the O_2-rich electrolyte flow-rate should be around 100 cc/sec/kw.

The total electrolyte flow rate should therefore amount to about 300 cc/sec/kw.

ii. Pressurization power requirements. The compressibility of 5 M KOH solution being about 25 x 10^{-6} atm^{-1}

(cf. Sec. III-1.d.), the energy E_c required to compress an initial electrolyte volume V_i at an initial pressure $p_i \simeq 10$ atm to a final volume V_f at a pressure $p_f \simeq 200$ atm is given by the relations:

$$E_c = \int_{p_i}^{p_f} p\,dV \qquad (7)$$

and

$$V \simeq V_i\left[1-\beta\,(p-p_i)\right] \qquad (8),$$

which yield

$$dV \simeq -\beta V_i\,dp \qquad (9)$$

$$E_c \simeq \beta V_i \int_{p_i}^{p_f} p\,dp \simeq \tfrac{1}{2}\beta V_i\,(p_f^2-p_i^2) \qquad (10)$$

$$\simeq \tfrac{1}{2} \times 25 \times 10^{-6}\ \text{atm}^{-1} \times (200\ \text{atm})^2 V_i$$

$$\simeq 0.5 V_i\ \text{atm}.$$

Hence, for $V_i \simeq 300$ cc, $E_c \simeq 150$ cc-atm $\simeq 15$ joules. The total pressurization power requirements amount therefore to around 15 w/kw or around 1.5% of the power output.

Actually, part of the pressurization power will be contributed by the vaporization of the reactants injected into the chamber. The specific volumes of H_2 and O_2 at 75 °C and 200 atm being 158 cc/mole and 141 cc/mole, respectively, the total contribution from reactant expansion would be of the order of

$$100\ \text{atm} \times 150\ \text{cc-mole}^{-1} \times (4.7 + 2.4) \times 10^{-3}\ \text{mole/sec} \simeq$$

$$100\ \text{cc-atm/sec} \simeq 10\ \text{watts}$$

per kw power output if the reactants were allowed to vaporize. However, dissolution of reactants in the electrolyte introduces a large uncertainty in the actual contribution to be expected from the partial reactant pressures. In any event, the total power required for adequate pressurization of the electrolyte-reactant mixture during the saturation step would not exceed the above-estimated value of 1.5% and may actually amount to less than 1% of the total power output.

d. Recompression of Expanded Gas

The gases leaving the cryogenic storage tanks and/or any gas-liquid separators may either be fed into a conventional low-pressure fuel cell or else be recompressed and injected into the pressurization chambers. The latter approach would dispose of any auxiliary fuel cell requirements provided that the mass of gas to be recompressed can be held down to a reasonable fraction f_g of the mass of reactants consumed. The energy required to recompress 1 gm-equivalent of each of the reactants from 3 atm to 200 atm would be approximately

$$(\tfrac{1}{1} + \tfrac{1}{2})0.030 \text{ F-v} \times \ln(200/3) \simeq 0.094 \text{ F-v},$$

which is less than 9% of the energy derivable from a fuel cell output of 1.1 v. With proper insulation of the cryogenic reactant system and with adequate precautions to minimize the concentration of gas-bubble nuclei in the electrolyte system, there seems to be no reason to expect a gas fraction f_g higher than 10%. Hence, any recompression power would amount to less than 0.1 x 9% = 0.9% of the power output.

e. Electrolyte Pumping Power

i. Flow velocities and pressure drops through the electrode pores. With the baffle arrangement of Fig. 5, the electrolyte must pass through two electrode thicknesses and be distributed on each pass over only half of the total electrode area, i.e., over 1800 cm^2 for a 1-kw fuel cell (cf. Sec. III-4.b.).

The H_2-rich electrolyte flow of 200 cc/sec per kw power output (cf. Sec. III-3.c.i.) must therefore yield an apparent flow velocity of 200 cm^3-sec^{-1}/1800 cm^2 ≃ 0.111 cm/sec.

The pressure drop through the anode may be estimated from Leva's correlation for fluid flow through fixed packings (42, 43):

$$P = \lambda \frac{L}{d_e} \frac{W_f^2 \gamma_m}{2g} \left[\frac{(1-f_p)^{3-n}}{f_p^3} \phi^{3-n} \right] \qquad (11),$$

where $\lambda = f_1(Re)$, is given by a graph in ref. 43,

$Re = Wd_{e.h.}/\nu$

$W = W_f/f_p$ = mean stream velocity in interstices between particles, in m/sec

W_f = stream velocity based on total cross-section area, m/sec

f_p = porosity

$d_{e.h.} = (2/3)f_p/(1-f_p)\phi_1 d_e$

$\phi_1 = \left[0.205 S_p V_p^{-2/3}\right]^{\frac{1}{2}}$ = particle shape factor

S_p = particle surface area, m^2

V_p = particle volume, m^3

d_e = diameter of sphere equivalent to packed particle in volume = $(6V/\pi)^{1/3}$

ν = kinematic viscosity, m^2/sec

L = bed length, m

γ_m = fluid density, kg/m^3

g = acceleration of gravity, m/sec^2

$\phi = \phi_1^2$, and

$n = f_2(Re)$, is also given by a graph (42, 43).

Setting, $W_f = 1.11 \times 10^{-3}$ m/sec, $d_e \simeq 10^{-6}$ m, $f_p \simeq 0.6$, $\phi_1 \simeq 1.2$, and $\nu \simeq 5 \times 10^{-7}$ m^2/sec, one obtains $d_{e.h.} \simeq 2/3 \times 0.6/(1-0.6) \times 1.2 \times 10^{-6}$ m $\simeq 1.2 \times 10^{-6}$ m,

$$Re \simeq \frac{1.11 \times 10^{-3}}{0.6} \text{ m/sec} \times \frac{1.2 \times 10^{-6} \text{ m}}{5 \times 10^{-7} \text{ m}^2/\text{sec}} \simeq 4.44 \times 10^{-3},$$

which yields $\lambda \simeq 8 \times 10^4$ and n = 1. Hence, for two anode thicknesses of 2.5×10^{-5} m each, the total pressure drop becomes

$$P_{anodes} \simeq 8 \times 10^4 \frac{2 \times 2.5 \times 10^{-5} \text{ m}}{10^{-6} \text{ m}} \frac{(1.11 \times 10^{-3} \text{ m/sec})^2}{2 \times 9.8 \text{ m/sec}^2} \times$$

$$1.2 \times 10^3 \text{kg/m}^3 \times \left(\frac{1.44}{1.5}\right)^3$$

$$\simeq 270 \text{ kg/m}^2 \simeq 0.027 \text{ atm.}$$

Similarly, the total cathodic electrolyte flow rate of 100 cm^3/sec per kw output (cf. Sec. III-3.c.i.) yields an apparent velocity of 100 $cm^3\text{-sec}^{-1}/1800$ $cm^2 \simeq 5.56 \times 10^{-4}$ m/sec = W_f. Hence,

$$Re \simeq \frac{6.67 \times 10^{-4} \text{ m-sec}^{-1} \times 1.2 \times 10^{-6} \text{ m}}{5 \times 10^{-7} \text{ m}^2/\text{sec}} \simeq 1.6 \times 10^{-3},$$

which yields $\lambda \simeq 3 \times 10^5$. Thus, the pressure drop through two cathode thicknesses of 0.01 cm each becomes

$$\Delta P_{cat} \simeq 3 \times 10^5 \times \frac{2 \times 10^{-4} \text{ m}}{10^{-6} \text{ m}} \times \frac{(5.56 \times 10^{-4} \text{ m/sec})^2}{2 \times 9.8 \text{ m/sec}^2} \times$$

$$1.2 \times 10^3 \text{kg/m}^3 \times \left(\frac{1.44}{1.5}\right)^3 \simeq 10^3 \text{ kg/m}^2 \simeq 0.1 \text{ atm.}$$

That the above pressure drop estimates are realistic may be ascertained from available specifications for Lockheed microporous stainless steel filters (44), according to which 0.025 cm thick Type E-300 filters with a particle

retention size of 0.7 micron would require a ΔP of around 0.2 atm for a room temperature water flow rate of 0.06 cm/sec, whereas comparable 1-micron size filters require only 0.07 atm for the same flow rate. These figures are surprisingly close to the above estimated ΔP_{cat} of 0.1 atm for a double cathode thickness of 0.020 cm.

From the preceding estimates it is evident that the average pressure drop per unit electrolyte volume for the combined anodic and cathodic flows, would amount to only

$$\Delta P_{av} \simeq \frac{200 \text{ cc} \times 0.027 \text{ atm} + 100 \text{ cc} \times 0.1 \text{ atm}}{300 \text{ cc}} \simeq 0.051 \text{ atm.}$$

This ΔP_{av} could, of course, be further reduced by increasing the average particle size and/or interspersing large diameter pores through the fine pore structure. Alternately, the average particle size can be greatly reduced without markedly increasing ΔP_{av} provided that pores in excess of 1 micron be interspersed throughout the electrodes.

ii. Total pressure drop and pumping power. It is easy to ascertain that the pressure drops through the channels adjoining the electrodes and also through the remainder of the electrolyte circulating system are small in comparison with the above-estimated $\Delta P_{av} \simeq 0.05$ atm. Hence a total effective pressure drop $\Delta P_T \simeq 0.1$ atm should

suffice to account for all these additional losses as well as for all expected pumping inefficiencies.

Hence, the electrolyte pumping power need not exceed 0.1 atm x 300 cc/sec = 30 cc-atm/sec ≃ 3 watts per kw power output, or 0.3% of total output.

f. Maximum Total Pumping and Pressurization Power Consumption

The above-estimated power requirements add up as follows:

Cryogenic pumping power	0.4% of output power
Pressurization of saturation chambers	<1.5% " " "
Recompression of expanded gas	<0.9% " " "
Electrolyte circulation	0.3% " " "
Total	<3.1% " " "

III-4. Fuel Cell Stack Analysis

a. Nominal Current Density

Assuming a shallow slope of the voltage-current density curves within the selected operating range, the main current density limitation would arise from ohmic losses through the electrolyte. Given an electrolyte resistivity $\rho \simeq 0.9$ ohm-cm (cf. Sec. III-1.b.) the spacings for the configuration of Fig. 5 as listed in Sec. II-2.b.i. ($L_a \simeq 0.0025$ cm, $L_g \simeq 0.01$ cm, $L_s \simeq 0.04$ cm, $L_c \simeq 0.01$ cm), and assuming that

f_t = tortuosity factor for electrode and separator matrix pores $\simeq 2$

f_e = fraction of total electrode thickness traversed by an average current flow-path $\simeq 0.5$, and

f_p = porosity of the electrode and separator structures $\simeq 0.6$,

then the total effective electrolyte resistance per cm^2 electrode face area becomes

$$R_{eff} \simeq \rho \left[f_e f_t f_p^{-1} (L_a + L_c) + f_t f_p^{-1} L_s + 2L_g \right] \qquad (12)$$

$$\simeq 0.16 \text{ ohm-cm}^2.$$

Hence, in order to keep the average ohmic loss down to less than 0.04 v, the average operating current

density should not exceed 0.25 amp/cm^2. The latter value is therefore selected here as the nominal average current density. Of course, much higher peak current densities may still be allowed at a rather moderate loss in output voltage.

b. Total Electrode Area

For an average cell voltage of 1.1 v (cf. Sec. III-4.iv.) and a current density of 0.25 amp/cm^2, the total electrode area per kw becomes

$$A_e \simeq \frac{10^3 \text{ v-amp}}{1.1 \text{ v} \times 0.25 \text{ amp/cm}^2} \simeq 3{,}600 \text{ cm}^2.$$

c. Electrode Thicknesses

By dispensing with binders, water repellants, and other extraneous materials the electrodes can be made much thinner than at present and yet provide a comparable catalyst area. E.g., a pure 60% porous sintered Pt or Raney Pt electrode comprising the same form and amount of Pt black as is currently used in the "high-loading" electrode type (45), i.e., 40 mg Pt/cm^2 apparent area, would have a thickness of only

$$\frac{0.040 \text{ gm/cm}^2}{(1-0.6)21.5 \text{ gm/cm}^3} \simeq 0.005 \text{ cm}.$$

An amount of Pt black comparable to that in "standard" electrodes, i.e., 9 mg/cm^2 (45), would require a thickness of only 0.001 cm.

Since the "standard" H_2 electrodes yield negligible polarization, i.e., 0.03-0.05 v at 0.2 amp/cm^2 at 30 ^oC (46), a thickness of 10^{-3} cm might be adequate for pure Pt anodes. However, to provide greater mechanical strength and maximum reliability against catalyst deterioration an anode thickness of 0.0025 cm is proposed here.

Similarly, a cathode thickness of 0.01 cm has been tentatively selected so as to yield at least a two-fold greater catalyst area than that provided by the above-cited "high-loading" electrodes.

d. Polarization and Ohmic Losses, and Net Cell Voltage

i. Absence of significant diffusion limitations and negligible anode polarization. In view of the relatively high exchange current density for the anodic reaction ($i_o \simeq 10^{-3}$ amp/cm^2), the selected anode thickness of 0.0025 cm may be at least an order of magnitude greater than required to ensure negligible activation polarization (9, 23).

To ascertain that diffusion polarization losses should also be negligible one can again apply the Einstein

relation (cf. Eq. (3), Sec. II-2.a.). Assuming an average pore diameter $d_p \simeq 10^{-4}$ cm, the average maximum radial distance $\bar{d}_m$ from the center of a pore to the pore wall becomes

$$\bar{d}_m \simeq \tfrac{1}{2} d_p \simeq 5 \times 10^{-5} \text{ cm} \qquad (13),$$

which, together with Eqs. (3) and (4), yields a maximum diffusion time

$$t_d \leq \bar{d}_m^2/2D \qquad (14)$$

$$\leq d_p^2/8D \qquad (15).$$

Hence, for $D_{H_2} \simeq 3 \times 10^{-5}$ cm^2/sec (cf. Sec. III-1.c.), one obtains

$$t_d \leq (10^{-4} \text{ cm})^2/(8 \times 3 \times 10^{-5} \text{ cm}^2/\text{sec}) \simeq 4 \times 10^{-5} \text{ sec},$$

as compared with a transit time through a single anode thickness of 0.0025 cm/0.111 cm-sec^{-1} $\simeq$ 0.023 sec. It is thus clear that the reactants should have ample time for diffusion to the pore walls.

The crude analysis based on Eq. (3), although far from rigorous, is believed to be more correct than those based on empirical correlations of effective mass transfer coefficients (22, 47), as the latter coefficients can only remain valid for substantial stagnant film thicknesses. When the pore diameters are so small that diffusion becomes quite rapid even in the absence of any

flow, the stagnant film concept and hence the correlations based thereon become meaningless, and can be replaced by a simpler analytical approach.

Moreover, since total anode polarization is known to be quite small (46) even under the relatively unfavorable conditions prevailing in gaseous diffusion electrodes (cf. Sec. I-1), it should become altogether negligible with the fast transport rate provided by the supersaturated electrode feed.

ii. Activation polarization at the cathode. Since the solubilities and diffusivities of O_2 and H_2 are comparable (cf. Sec. III-1.a. and c.) and only $\frac{1}{2}$ mole O_2 is required per mole of H_2, diffusion polarization should be a fortiori negligible at the cathodes, especially in view of the four-fold greater cathode thickness (or longer transit time through the cathode pores). The chief remaining rate limitation must therefore be associated with activation polarization at the cathode (23, 46).

It might be tempting to apply here the results of several pertinent theoretical analyses (48-50). Indeed with the baffle arrangement of Fig. 5, the electrolyte enters from the back through one half of the electrode area and from the front through the other half. Hence, the analytical solutions worked out for flooded-flow

electrodes with posterior and frontal reactant feeds should be applicable in this case. However, these solutions can not be used to predict electrode polarization without reliable data for the exchange current density at O_2 electrodes in the 75 °C-100 °C range. A more empirical and simpler approach must therefore be resorted to.

Given the polarization curves for porous diffusion type fuel cells at atmospheric pressure and 70 °C with 5 M KOH (45, 46), it may suffice to estimate the apparent current density i_{GD} at the tested gas-diffusion electrodes which may produce the same activation polarization as that of a supersaturated-feed electrode operating at the apparent current density i_{SF}. The ratio of i_{SF} to i_{GD} should be proportional to the ratios of the respective catalyst surface areas A_{SF}/A_{GD} and of the respective exchange current densities $i_{o_{SF}}/i_{o_{GD}}$, i.e.,

$$i_{SF}/i_{GD} \simeq (A_{SF}/A_{GD})\ (i_{o_{SF}}/i_{o_{GD}}) \qquad (16).$$

Now, i_o is known to increase with increasing reactant concentration at the electrode surface (4, 7, 51-53). E.g., an increase in O_2 pressure in the range of 1-100 atm on Pt electrodes translates the Tafel curve "towards

increasing current in amount directly proportional to the oxygen pressure" (ref. 53, pp. 21 and 24). Even after making allowance for the expected increase in open-circuit potential (cf. Eq. (1), Sec I-6), the measured translation still appears proportional to at least $p_{O_2}^{2/3} \simeq 34$. Furthermore, a cathode thickness of 0.010 cm was shown in Sec. III-4.c. to yield at least twice the catalyst surface area as that provided by a "high-loading" electrode. Hence, $i_{SF}/i_{GD} \simeq 2 \times 34 \simeq 68$, i.e., an i_{SF} of 0.25 amp/cm^2 should result in the same activation overvoltage as that observed for $i_{GD} \simeq 0.004$ amp/cm^2.

With 5 M KOH at 70 °C and 1 atm, the working cell voltage corresponding to $i_{GD} \simeq 0.005$ amp/cm^2 is at least 1.0 v (ref. 45, Fig. 3), as compared with an observed mixed open-circuit potential of 1.05 v (45) and a theoretical e.m.f. of 1.19 v (25). Hence, cathode polarization with supersaturated feed should not exceed 0.19 v with respect to the theoretical emf or 0.05 v with respect to the actual open-circuit voltage.

iii. Total polarization and ohmic losses. The maximum polarization loss of 0.19 v estimated in Sec. iii-4.d.ii. represents the sum total of all electrode polarization losses to be expected at the nominal current density of

0.25 amp/cm^2. Most of these losses are attributable to a mixed O_2-H_2O_2 potential at the cathode. In addition, the ohmic loss was estimated at 0.04 v for the same current density (cf. Sec. III-4.a.). Hence, the total polarization and ohmic losses should not exceed 0.19 v + 0.04 v = 0.23 v.

iv. Net cell output at nominal load. As pointed out in Sec. I-6, the theoretical emf should increase by 0.12 v at 200 atm pressure with respect to the atmospheric value of 1.19 v. The total theoretical emf adds up then to 1.31 v. Subtracting the total losses estimated in Sec. III-4.d.iii., one obtains a net cell output at 0.25 amp/cm^2 of at least 1.31 v-0.23 v = 1.08 v. Moreover, in view of several other favorable factors excluded from the above estimates for the sake of simplicity, it appears safe to conclude that the actual operating voltage should easily exceed 1.10 v.

III-5. Bubble Nucleation and Growth Rate

a. Requirements for Negligible Gas Evolution

The mechanism of any phase transition is known to be initiated by the formation of stable nuclei of a critical minimum size and to be followed by the growth and multiplication of nuclei (54-56). Nuclear growth is limited by the rate of diffusion of

solute molecules toward the stable nuclei. Hence, the condition for negligible gassing is that the mean time t_{gb} for diffusion to a stable gas bubble be much longer than the total transit time t_T through an electrolyte circulation loop. More exactly, the transit time from the saturation chamber to the fuel cell outlets t_{fo} should be less than 0.1 t_{gb} if the evolved gas is not to exceed a fraction f_g greater than 10% of the amount consumed at the electrodes:

$$t_{fo} < 0.1\ t_{gb} \qquad (17).$$

Now the apparent flow velocity through the cathodes was estimated in Sec. III-3.e.i. at 0.056 cm/sec. Hence the transit time through two cathode thicknesses would alone amount to 0.02 cm/0.056 cm-sec^{-1} $\simeq$ 0.36 sec. Hence t_{fo} must be of the order of $\frac{1}{2}$ sec during operation at nominal load, and t_{gb} must accordingly exceed 5 sec. Therefore according to Eq. (3), the mean distance d_{gb} to a gas bubble nucleus should be at least

$$d_{gb} \geq (2Dt_{gb})^{\frac{1}{2}} \geq (2 \times 3 \times 10^{-5}\ \text{cm}^2\text{-sec}^{-1} \times 5\ \text{sec})^{\frac{1}{2}} \simeq 0.02\ \text{cm}.$$

Hence, the concentration of gas nuclei must be kept down to less than $(0.02\ \text{cm})^{-3} \simeq 10^5\ \text{cm}^{-3}$.

Whether this condition can be easily satisfied will depend on the prevailing nucleation mechanism.

b. Homogeneous Nucleation

Homogeneous nucleation is expected to occur only when the ratio of the nucleating solute pressure p_n to its equilibrium pressure p_e approaches the Volmer relation (54-56)

$$\ln(p_n/p_e) = (16\pi\sigma^3 V_m^2/3k^3T^3 \ln C)^{\frac{1}{2}} \qquad (18),$$

where σ is the interfacial tension, V_m is the molecular volume of the solute, k is Boltzmann's constant, T is the absolute temperature, and C is a constant approximately equal to 10^{25} (55). The surface tension σ of 5 M KOH at 75 °C being around 70 dynes/cm, and setting p_e = 10 atm, and $V_m/kT \simeq p_e^{-1}$ for gas bubbles, one obtains

$$\ln(p_n/p_e) \simeq (16\pi 70^3 \text{ dyne}^3\text{-cm}^{-3} \times 10^{-2} \text{ atm}^{-2}/3kT \ln 10^{25})^{\frac{1}{2}}$$
$$\simeq 140,$$

which would require a pressure $p_n \simeq 10^{63}$ atm in order for homogeneous nucleation to occur. Alternately, according to a somewhat different version of the Volmer relation (ref. 56, p. 16) the rate of homogeneous nucleation at a saturation ratio of 200 atm/10 atm = 20 would be of the order of $10^{-3,700}$ cm^{-3}-sec^{-1}. It appears therefore that no degassing would be encountered in the absence of foreign nuclei.

c. Heterogeneous Nucleation

To prevent or minimize heterogeneous nucleation a few rather simple precautions may have to be taken. In the first place, cleanliness of the electrolyte and thorough wetting of the entire electrolyte circulation system should be of major importance. According to Walton (55), it has been possible to heat water as high as 200 ^{o}C without boiling by paying thorough attention to purity and to perfect wetting of the container walls. In contrast, Hummel and Young have succeeded in greatly accelerating the nucleation of bubbles on heated metal by depositing a multitude of tiny Teflon spots on the heated surface (55). Tiny Teflon particles would therefore have to be definitely kept out of the electrolyte circulation system.

It may also be necessary to minimize shock or spurious vibrations by providing shock dampeners in or around those parts of the electrolyte system which are outside the saturation chambers, as pressure waves are known to accelerate nucleation (55). Finally, it may be desirable to condition the electrolyte system with a stable electrochemically harmless surface wetting additive.

By means of such precautions it would not seem difficult to keep the bubble nuclei far below the maximum allowable concentration of 10^{5} cm^{-3} (cf. Sec. III-5.a.).

IV. WEIGHT ESTIMATES

Any weight assessment for an entire supersaturated feed fuel cell system (SFFC) could not be exact in the absence of detailed mechanical designs going far beyond the scope of this study. The present estimates will therefore be restricted to the major differences between the SFFC and the gaseous-diffusion type (GDT) systems.

The weights of the additional components required by the SFFC but not by the GDT are first estimated in Sec. IV-1. The savings in fuel stack, radiator, reactant, and storage tank weights are then computed in Secs. IV-2, IV-3, and IV-4, and the net savings derived from the SFFC are summed up in Sec. IV-5. Since the component weights of Sec. IV-1 are the most difficult to assess accurately, special pains have been taken to lean toward the conservative direction, so that the component weight of Sec. IV-1 may be far higher than required and the net savings of Sec. IV-5 considerably lower than what may be realized.

IV-1. Extra Component Weights

The extra weight of the additional required components can be only roughly estimated from that of similar hardware commercially available at present. Furthermore, the incremental weight requirements per kw power output may be expected to decrease with increasing power capacity. The present estimates will therefore start with a minimum nominal power output of 2 kw, as a basis. Of the total extra component weight W_c estimated for the minimum size, half will be assumed to constitute a fixed minimum W_m, and half will be assumed to be proportional to the fuel cell power, P_F:

$$W_c \simeq W_m + F_p P_F \qquad (19)$$

where the proportionality factor F_p would be derived from the relation

$$\tfrac{1}{2}(W_c)_{2KW} \simeq 2F_p \text{ lb-kw}^{-1} \qquad (20).$$

To estimate $(W_c)_{2KW}$ one may start first with the saturation chamber weights W_s, which should not exceed 1 lb/100 cc (cf. Sec. II-2.a.), i.e., 3 lb for a total chamber capacity of 300 cc (200 cc and 100 cc for the H_2-rich and O_2-rich electrolytes, respectively). In addition, each chamber requires 3 automatically actuated valves capable of withstanding a maximum back-pressure of 200 atm, including one fast-response cryogenic valve operating at a high pressure differential, and two simultaneously acting valves subjected to a negligible pressure differential when open. The latter two valves can be

replaced by a single double-acting valve weighing around 1 lb, while the single cryogenic valve might weigh around ½ lb (including insulation). The total saturation chamber weight including 2 cryogenic valves and 2 double-acting electrolyte valves may thus add up to

$$(W_s)_{2KW} \simeq 3 \text{ lb} + 2(1 \text{ lb} + \tfrac{1}{2} \text{ lb}) \simeq 6 \text{ lb}.$$

That the above valve weights are conservative may be seen from quotations for commercially available valves such as Circle Seal high-response solenoid valves Model V4149 or V4152, rated for pressures in excess of 3,000 psi and response times of 1 or 2 msec, described as "suitable for cryogenic service," and weighing only about ½ lb (57).

The micro-volume high-pressure cryogenic pumps required to inject 0.13 cc H_2 and 0.07 cc O_2 per cycle or per kw-sec (cf. Sec. III-3.b.) might be compared with an Eastern size 102 hydraulic pump (58) capable of delivering around 1½ gpm (or almost 100 cc/sec) at 100 atm, and weighing only 1.6 lb (without motor). Hence, in view of the much smaller volume requirements (0.26 cc H_2/sec or 0.14 cc O_2/sec for operation at 2 kw), a weight of 1.3 lb for the liquid H_2 pump and of 0.7 lb for the liquid O_2 pump, including insulation and subcooling chambers,

appears to be a conservative estimate. The total weight W_L of the liquid reactant pumping system may thus add up to

$$(W_L)_{2KW} \simeq 1.3 \text{ lb} + 0.7 \text{ lb} \simeq 2 \text{ lb}.$$

The electrolyte pumps may be compared with an Eastern Industries Type VO-2100 (58) weighing $1\frac{1}{2}$ lb (without motor) and delivering around 9 gpm (500 cc/sec) at 10 atm discharge pressure. Hence, assuming that one such pump may be required for each of the O_2-rich and H_2-rich electrolyte lines, the total weight W_E of the electrolyte pumps would add up to

$$(W_E)_{2KW} \simeq 3 \text{ lb}.$$

In view of the relatively small auxiliary power requirements (3% of 2 KW $\simeq$ 60 watts), the weights of motors and controls, W_{MC}, should not exceed 2 lb,

$$(W_{MC})_{2KW} \simeq 2 \text{ lb}.$$

Similarly, the additional hardware required to convert the already existing heat-rejection system into a 100- to 200-watt thermal engine should not exceed $(W_{Th})_{2KW} \simeq 3$ lb.

Although each of these estimated component weights may be too conservative (cf. Sec. II-3.a.), their sum total is only

$$(W_c)_{2KW} \simeq (W_s + W_L + W_E + W_{MC} + W_{Th})_{2KW}$$
$$(6 + 2 + 3 + 2 + 3)\ \text{lb} \simeq 16\ \text{lb}.$$

Hence, Eqs. (19) and (20) assume the approximate form

$$W_c \simeq 4\ \text{lb} + 4\ P_F\ \text{lb-kw}^{-1} \qquad (21).$$

Thus, for nominal fuel cell powers P_F of 5 kw, 10 kw, and 20 kw the estimated W_c would be around 24 lb, 44 lb, and 84 lb. In the 20-50 KW range the rate of increase in W_c should be somewhat slower, i.e., W_c may amount to around 150 lb for a 50-kw system. All of these values are probably at least twice as high as what may be actually required, but they may still permit a meaningful comparison with alternate systems.

IV-2. Saving in Cell Stack Weight

A currently available 2-kw fuel cell system weighs 100-140 lb/kw of sustained power when filled with electrolyte and operating at a current density of 100 amps/ft^2 (11, 59). Although this weight might be considerably reduced with moderate state-of-the-art advances, the minimum weight of the gas-diffusion type fuel cell stacks alone could not be less than the 20 lb/kw presently obtainable at peak power (59).

On the other hand, with the cell dimensions proposed

in Sec. II-2.b.i., the active fuel cell volume would be only around

$$0.123 \text{ cm} \times 3{,}600 \text{ cm}^2/\text{kw} \simeq 440 \text{ cm}^3/\text{kw},$$

of which only 10% would consist of the relatively heavy porous electrode volume. The density of Pt being 21.45 gm/cm^3, even a 60% porous electrode would have an effective density of $(0.4 \times 21.5 + 0.6 \times 1.2)$ $\text{gm/cm}^3 \simeq 9.3$ gm/cm^3 when filled with electrolyte. Assuming an average density of 2 gm/cm^3 for the electrolyte, separator, and cell wall materials, the weight W_a of the active cell volume becomes

$$W_a \simeq 440 \text{ cm}^3 \, (0.10 \times 9.3 \text{ gm/cm}^3 + 0.90 \times 2 \text{ gm/cm}^3)/\text{kw}$$
$$\simeq 2.7 \text{ lb/kw}.$$

In addition, the cell edges, gaskets, manifolds, end-plates, inlet-outlet tubing, and the electrolyte contained in the circulating system may double the above weight for a total fuel cell and electrolyte weight

$$W_{FE} \simeq 5.4 \text{ lb/kw}.$$

Hence, even assuming the minimum achievable weight of 20 lb/kw for gas diffusion type fuel cell stacks, one would still expect a weight saving W_{SF} of around 15 lb/kw in cell stack weight:

$$W_{SF} \simeq 15 \, P_F \text{ lb-kw}^{-1} \qquad (22).$$

According to Eqs. (21) and (22), W_{SF} would alone suffice to cancel out W_c and yield a net saving in total

equipment weight even for P_F = 2 kw. This conclusion is in at least qualitative agreement with the results of Reti and Sadek (23).

IV-3. Saving in Radiator Weight

The radiator used with present GDT fuel cell systems weighs 20 to 25 lb/kw electrical power output (59). With the higher energy conversion efficiency of the SFFC the reduced heat rejection requirements should permit a proportionate decrease in radiator weight. At an output of 1.1 v/cell the SFFC heat production rate was found to amount to 430 w/kw (cf. Sec. II-2.c.). In present GDT fuel cells operating at 0.90 v/cell, the heat production rate must amount to 0.57 v/0.90 v $\simeq$ 63% or 630 w/kw. The required radiator weight is thus reduced by (63%-43%)/63% $\simeq$ 32% for otherwise identical cooling conditions. Thus, assuming the lower limit of 20 lb/kw for the weight of present radiators, the net saving in radiator weight becomes

$$W_{SRad} \simeq 0.3 \times 20 \text{ lb-kw}^{-1} \simeq 6 \text{ lb-kw}^{-1} \quad (23).$$

IV-4. Savings in Reactant and Tank Weights

At 0.90 volt/cell and 100% Faradaic efficiency, the total reactant consumption amounts to 0.82 lb/kw-hr.

The ratio of storage tank weight to reactant weight being around 2/3 (59), the total required reactant and tank weight would add up then to around 1.37 lb/kw-hr.

This weight requirement would decrease in inverse proportion to the cell voltage, thus reducing to (0.9/1.1) x 1.37 lb/kw-hr ≃ 1.12 lb/kw-hr for a system operating at 1.1 volt/cell and 100% Faradaic efficiency. The net saving W_{SR} in total reactant and tank weights is therefore

$$W_{SR} \simeq (1.37\text{-}1.12) \text{ lb/kw-hr} \simeq 0.25 \text{ lb/kw-hr}.$$

Setting t_p for the time of continuous operation at the rated power P_F, one can express this result in the form

$$W_{SR} = 0.25\ t_p P_F \text{ lb-kw}^{-1}\text{-hr}^{-1} \qquad (24).$$

IV-5. Over-all Weight Saving

Combining Eqs. (21) through (24), one obtains an over-all net weight saving

$$W_{SN} \simeq (0.25 t_p \text{ hr}^{-1} + 17) P_F \text{ lb-kw}^{-1} - 4 \text{ lb} \qquad (25).$$

A net saving is thus expected even for P_F as low as 1 KW in missions of short duration. For missions of more than 60 hr the savings in reactant and tank weights become predominant, as shown graphically in Fig. 6.

V. ADJUSTMENT TO VARIABLE LOAD AND MISSION REQUIREMENTS

V-1. System Simplifications for Missions of Short Duration

The design and weight estimates of Secs. II and III were primarily concerned with operation at or near maximum energy conversion efficiency. Such maximum efficiency operation would be most desirable for missions of long duration, e.g., of more than 60 hr, where the savings in reactant and storage tank weights become the predominant factor (cf. Sec. IV-4). However, for shorter missions, it may be advantageous to minimize equipment weight even at an appreciable sacrifice of reactant consumption efficiency. For such missions the SFFC system could be simplified and/or made considerably lighter by elimination of any auxiliary GDT fuel cell and/or of the thermal engine and by further reduction in fuel cell stack weight by operation at higher current densities, i.e., closer to the peak power capability limits arrived at in Sec. V-3. Without the thermal engine the radiator temperature could be raised to 340 ^{o}K or higher, which could cut down the radiator weight almost in half. Around 10 lb/kw could thus be saved in toto by operating the fuel cell stack at twice its rated power. A further saving of 3 lb/kw could then be realized on the radiator weight by allowing the water product to evaporate directly into empty space.

V-2. Stand-By or Low Power Operation

Although a downward or upward factor of around 4 was assumed in Sec. II-2.a. to be the maximum desirable deviation from rated power (more exactly 0.5 to 10 kw for a nominal 2-kw system), low power operation or even stand-by readiness could be maintained, nevertheless, if need be, at a relatively low rate of reactant consumption.

In the absence of significant reactant diffusion through the separator matrix, the SFFC could be maintained in permanent stand-by readiness even without any power consumption, as the partial reactant pressures of 10 atm in a completely equilibrated system could still yield sufficient fuel cell power to bring the system into immediate operation. Since the actual reactant diffusion rate through a tight 0.04 cm thick separator matrix would amount to far less than 0.1% of the rate of consumption at nominal load, and the parasitic power demands are also insignificant in the absence of power drain, the total reactant consumption rate under no load conditions should be considerably less than 0.1% of the average operating rate.

V-3. Peak Power Capability

As suggested in Sec. II-2.a., a peak power capability

of around 5 times the rated load should be feasible by increasing the saturation cycle frequency in roughly the same proportion. However, at a 5-fold increase in current density relative to the nominal value of 0.25 amps/cm^2, the ohmic and polarization losses would be increased by around 0.20 v (cf. Secs. II-4.a. and d.). The actual power gain would then amount to a factor of only 5 x 0.90 v/1.10 v $\simeq$ 4.1. An 8-fold increase in current density would reduce the operating voltage to around 0.75 v/cell and thus yield a peak power of 8 x 0.75 v/1.1 v $\simeq$ 5.5 times the rated load. The peak power capability should therefore be in the range of 4 to 6 times the nominal power.

V-4. Sensitivity to Overloads

At any given cycling frequency the continuous current drawn from the SFFC could not exceed the limit determined by the rate of reactant transport. It is thus possible to prevent any dangerous overload by limiting the operational frequency range of the controlling oscillator (cf. Sec. II-3.b.iii).

Even in case of malfunction of the frequency limiting provision, the following operative mechanisms would serve to prevent any serious overheat damage to the fuel cell stack:

a. Increased cycling frequency and electrolyte temperature would result in an increased heat removal rate.

b. Increased electrolyte temperature would result in lower reactant solubilities and hence higher cycling and cooling rates for a given current drain.

c. Increased electrolyte temperature would also result in reduced ohmic and polarization losses and hence reduced heat generation rate.

It would thus be rather difficult to effect any damage in the SFFC stacks through electrical overloads. Of course, the possibility may arise of mechanical damage to the accessory components at excessive cycling frequencies. However, such damage could be prevented by selecting or designing components rated for at least 10 times the maximum expected cycling frequency.

VI. OVER-ALL ASSESSMENT OF THE SUPERSATURATED FEED APPROACH

VI-1. Comparison with Gaseous Fuel Cells

According to Eq (25), Sec. IV-5, the SFFC system should result in net savings of around 17 lb/kw in equipment weight alone and of $\frac{1}{4}$ lb/kw-hr in the weight of reactants and tanks. This yields total savings of 42 lb/kw and 267 lb/kw for 100-hr and 1,000-hr missions, respectively. A saving of about a ton is realized on an 8,000 kw-hr system.

On missions of short duration the savings in reactant weights become insignificant, but the accessory equipment may then be greatly simplified so as to yield further savings of around 13 lb/kw (cf. Sec. V-1). The total savings in equipment weight would then amount to 30 lb/kw. Since the total weight of GDT systems may be reduced to under 100 lb/kw with moderate state-of-the-art improvements (59), these estimated savings would amount to an overall reduction of at least 30% over the minimum that might be achieved with GDT systems.

Since the savings in reactant and tank weights during longer missions would also amount to over 20% of the minimum required with GDT systems, the over-all weight savings realizable with an SFFC should amount to at least 20-30% regardless of mission length.

The savings in equipment arise chiefly from the major size reductions in the fuel cell stack and in the radiator permitted by increased energy efficiency and power capability.

Yet, even with the major reduction in cell stack size, the peak power capability is around 4 to 6 times the rated power with the SFFC system, whereas a peak to average power ratio of 2:1 is barely achievable with the GDT (11). Neither should the SFFC stacks be subject to the gradual deterioration observed with the GDT (11, 12).

The only objectionable feature of the SFFC system may be the requirement for accessory mechanical equipment involving moving parts. However, the number of such parts can be kept reasonably small through proper design. Moreover, any loss in reliability associated with such moving parts should be amply offset by the improved reliability of the fuel cell stack.

VI-2. Comparison with Undersaturated Flooded-Flow Systems

To determine whether the above-demonstrated advantages are due primarily to the supersaturated feed or to the flooded-flow approach a comparison with undersaturated flooded-flow (UFF) systems may be of interest.

The earlier UFF cells of Bacon (13) and Meissner and Reti (21, 22) have already been covered in Sec. I-2. However, the recent study of Reti and Sadek (23), hereafter referred to as R & S, calls for a closer comparison.

Both the present and the R & S studies agree at least qualitatively that:

a) the flooded-flow approach offers significant advantages over GDT fuel cells;

b) this approach calls for saturation pressures of at least 50 atm and preferably higher pressures; and

c) this approach results in considerable savings in over-all equipment weight alone.

However, R & S obtain no gain in over-all energy efficiency and hence no savings in reactant weights. Neither do these studies agree quantitatively on several major points.

An absolute weight comparison between the SFFC discussed here and the UFF system of R & S is not possible because the weights estimated in Sec. IV for comparable equipment are clearly far more conservative than those of R & S. It is possible, however, to assess the relative advantage by referring consistently to the R & S weight estimates.

For mission lengths of 24 hr to 240 hr R & S arrive

at an optimized equipment weight breakdown of around 5-6 lb for the fuel cell stack, 12-13 lb for the radiator, and 9-10 lb for the saturators per kw power output. These equipment weights should be reduced by the following percentages with the SFFC system presented in Secs. II and III:

a) a reduction of at least 40-60% in fuel cell stack arising from higher current density (0.25 amp/cm^2 as compared with 0.13-0.18 amp/cm^2) and higher voltage output (1.1 v/cell as compared with 0.85-0.87 v/cell);

b) a reduction of at least 40% in radiator weight arising from reduced heat generation at higher output voltage (cf. Sec. IV-3); and

c) a reduction of at least 50% in saturator weight arising from reduced saturator volume and reduced pumping requirements with higher saturation pressures.

The SFFC approach results therefore in an equipment weight reduction of around 50% and in a reactant weight reduction of (1.10 v-0.87 v)/0.87 v $\simeq$ 26%.

The rather low voltage output arrived at by R & S appears to result partly from low temperature operation, and the ohmic and polarization losses associated therewith, and partly from the lower operating pressure which leads to higher polarization losses and higher parasitic power requirements. A higher operating temperature would result

in lower ohmic and polarization losses but in higher pumping requirements.

Neither could the UFF system proposed by R & S yield the high peak power capabilities of the SFFC (cf. Sec. V-3) since their pumping requirements are rather high even at rated load.

It should, of course, be possible to introduce certain improvements in the UFF system which may narrow down these differences somewhat. E.g., by operating the UFF system at 200 atm and 75 ^{o}C the savings in reactant and tank weights obtained with the SFFC should also be realized with the UFF. However, the total equipment weight would then have to be increased considerably, as the entire system would have to withstand at least 200 atm pressure. Even the saturation chambers would have to be increased appreciably since it would not be easy to inject a cryogenic reactant spray through high-pressure nozzles into an already pressurized electrolyte.

The major gains arrived at in this study appear therefore to derive chiefly from the supersaturation approach.

VII. CONCLUSIONS

The over-all weight savings of at least 20% obtained with the SFFC as compared with either the GDT or the UFF systems derive chiefly from the attainment of high reactant activities in the circulating electrolytes. For the saturation pressures of 200 atm assumed in this study, the weight of accessory equipment and the pumping and pressurization power requirements were found to be negligible in comparison with the over-all gains. Although further net gains may be realized with even higher saturation pressures, the optimum point would probably not exceed 600 atm, as the additional equipment weight and parasitic power requirements would then definitely begin to outweigh the marginal advantages to be gained from further pressure increases.

Further gains through reduced cathode polarization should result from higher operating temperatures, e.g., 100-150 ^{o}C. However, in the absence of reactant solubility data, the optimum temperature region remains uncertain.

The expected improvements in fuel cell performance may be large enough to elicit justifiable disbelief and a suspicion that the above estimates may have been somehow biased in favor of the SFFC. That is why considerable

pains have been taken throughout this work to take into account any possible problem areas and to discount several additional favorable factors. E.g., in the estimates of polarization losses (cf. Sec. III-4.d.) no allowance was made for the improved utilization of the available catalyst area arising from the absence of obstructions by gases, water-repellents or inactive binders. Also left unmentioned are the simplifications in electrode manufacture and the increased reliability obtainable with a pure porous catalyst structure, or the further weight savings realizable by dispensing with some of the accessories required with GDT systems, such as the heating elements and controls presently used to draw gaseous reactants from cryogenic tanks during peak power demand.

Further work aimed at demonstrating the advantages of SFFC in actual practice should start with the construction and testing of a small SFFC utilizing conventional saturation and pumping equipment. This could be followed first by the design, construction and testing of tailor-made accessory components, and finally by the construction, trouble-shooting, and life-testing of a complete system.

REFERENCES

1. C. Wagner, unpublished communication (1957).

2. H. C. Weber, H. P. Meissner, and D. A. Sama, J. Electrochem. Soc. 109, 884 (1962).

3. F. G. Will, Ibid. 110, 145 (1963); 110, 152 (1963); 114, 138 (1967).

4. R. P. Iczkowski, Ibid. 111, 605 (1964); 111, 1078 (1964).

5. T. Katan, S. Szpak, and E. A. Grens II, Ibid. 112, 1166 (1965).

6. J. A. Rockett and R. Brown, Ibid. 113, 207 (1966).

7. D. N. Bennion and Ch. W. Tobias, Ibid. 113, 589 (1966); 113, 593 (1966).

8. J. O'M. Bockris, "Studies in Fundamental Chemistry of Fuel Cell Reactions," Semi-Annual Report No. 9, Feb. 27, 1967, NSG-325, pp. 1-2.

9. B. D. Cahan and J. O'M. Bockris, Abstract No. 202, Extended Abstracts I-6, Electrochemical Society Meeting, May 7-12, 1967.

10. J. O'M. Bockris, L. Nanis, and B. D. Cahan, J. Electroanal.Chem. 9, 474 (1965).

11. J. L. Miller and J. F. Euclide, Paper No. 31PP66-508, AIEEE Meeting, New Orleans, July 12, 1966.

12. M. B. Clark and G. E. Evans, "Development of Fuel Cell Electrodes," Semi-Annual Report, Dec. 31, 1966, Contract NAS 3-9430, p. 48.

13. A. M. Adams, F. T. Bacon, and R. G. H. Watson in "Fuel Cells," edited by W. Mitchell, Jr. (Academic Press, New York, 1963), pp. 129-192, especially pp. 162-5.

14. G. Geffcken, Z. physik. Chemie 49, 257 (1904).

15. M. B. Knaster and L. A. Apelbaum, Zhur. Fiz. Khim. 38, 223 (1964); Russian J. Phys. Chem. 38, 120 (1964).

16. K. E. Gubbins and R. D. Walker, Jr., J. Electrochem. Soc. 112, 469 (1965).

17. R. D. Walker, Jr., "Study of Gas Solubility and Transport Properties in Fuel Cell Electrolytes," NASA Research Grant NGR 10-005-022, First Semi-Annual Report, March 15, 1966, pp. 4-9; Second Semi-Annual Report, Oct. 7, 1966, p. 14; Third Semi-Annual Report, March 29, 1967, pp. 18-25.

18. P. Ruetschi, and R. F. Amlie, J. Phys. Chem. 70, 718, (1966).

19. P. Ruetschi, J. Electrochem. Soc. 114, 301 (1967).

20. J. G. Tschinkel, internal report, Pratt & Whitney Aircraft.

21. H. P. Meissner and A. R. Reti in "Fuel Cells," Chem. Eng. Progr. Technical Manual, 40-44 (1963); also ASME Paper No. 63-WA-350 (1963).

22. A. R. Reti, Thesis, Massachusetts Institute of Technology (1962).

23. A. R. Reti and Sh. Sadek, "Use of Flow-Through Electrodes in a High Current Density Hydrogen-Oxygen Fuel Cell Stack," Final Report, June 12, 1967, Contract NAS7-530.

24. G. Eklund, unpublished report.

25. M. Eisenberg in "Fuel Cells," edited by W. Mitchell, Jr. (Academic Press, New York, 1963), pp. 17-64, especially pp. 47-50.

26. P. R. Schrantz, "Temperature Control of the Orbital Otolith Experiment," NASA CR-815, June 1967, p. 5.

27. J. Th. Taylor, "Thermal Control Considerations for a Manned Orbiting Space Station," NASA TN D-3995, May 1967, p. 39.

28. R. W. Graham and R. C. Hendricks, "Assessment of Convection, Conduction and Evaporation in Nucleate Boiling," NASA TN D-3943, May 1967.

29. Hoke Inc., Creskill, N. J. Catalog Sheet SC 76615.

30. F. T. Bacon in "Hydrocarbon Fuel Cell Technology," edited by B. S. Baker (Academic Press, New York, 1965), pp. 3-4.

31. A. Einstein, Ann. Physik 17, 549 (1905); 19, 371 (1906).

32. B. Brown and J. E. Goodman, "High-Intensity Ultrasonics" (D. Van Nostrand Company, Princeton, N. J., 1965), pp. 64-69, 136-159, 210-213, and 217-220.

33. P. R. Shipps, Proc. 20th Ann. Power Sources Conf. (PSC Publications, P.O. Box 891, Red Bank, N. J., 1966), pp. 86-88.

34. Th. H. Hacha et al. "Development of the Dual Membrane Fuel Cell and the Osmotic Still," Final Report, Contract NAS3-2551, January 15, 1964, pp. 154-200.

35. "Chemical Engineers' Handbook," edited by J. H. Perry (McGraw-Hill, New York, 1941).

36. F. A. Holland and F. S. Chapman, "Pumping of Liquids" (Reinhold, New York, 1966).

37. E. C. Fitch, Jr., "Fluid Power and Control Systems" (McGraw-Hill, New York, 1966).

38. "Lange's Handbook of Chemistry" (Handbook Publishers, Sandusky, Ohio, 1941).

39. R. W. Gurney, "Ionic Processes in Solution" (McGraw-Hill, New York, 1953), p. 69.

40. Ref. 13, p. 156.

41. H. S. Harned and B. B. Owen, "Physical Chemistry of Electrolyte Solutions" (Reinhold, New York, 1950), pp. 269-272.

42. M. Leva, Chem. Eng., Feb. 1957, pp. 263-8.

43. S. S. Zabrodsky, "Hydrodynamics and Heat Transfer in Fluidized Beds" (M.I.T. Press, Cambridge, Mass., 1966), pp. 2-3.

44. "Lockheed Development of Microporous Metal Media," Jan. 1967, anonymous brochure forwarded by C. G. Goetzel (Lockheed Company, Palo Alto, California), p. 4.

45. W. P. Colman, D. Gershberg, J. DiPalma, and R. G. Haldeman, Proc. 19th Ann. Power Sources Conf. (PSC Publications, 1965), pp. 14-17.

46. R. G. Haldeman, W. P. Colman, S. H. Langer, and W. A. Barber, Advances in Chemistry Series, No. 47, pp. 106-115 (1965).

47. S. G. Paradis, Thesis, M.I.T. (1966).

48. J. S. Newman and Ch. W. Tobias, J. Electrochem. Soc. 109, 1183 (1962).

49. L. G. Austin, P. Palasi, and R. R. Kimpel, 145th Am. Chem. Soc. Meeting, Div. of Fuel Chemistry, Preprints of Papers, Vol. 7, No. 4, pp. 48-83 (1963).

50. I. G. Gurevich and V. S. Bagotskii, in "Fuel Cells; Their Electrochemical Kinetics" edited by V. S. Bagotskii and Yu. B. Vasilev (Consultants Bureau, New York, 1966), pp. 47-75.

51. K. J. Vetter, "Electrochemical Kinetics" (Academic Press, New York, 1967), p. 117.

52. Ref. 13, pp. 141-144.

53. R. J. Bowen, H. B. Urbach, and J. H. Harrison, Electrochem. Soc. Meeting, May 1967, Abstract Nos. 169 and 170, Extended Abstracts I-6, Vol. 5, pp. 16-24.

54. M. Volmer, "Kinetik der Phasenbildung" (Stein, Dresden, 1934).

55. A. Walton, Int. Science & Technology, No. 60, pp. 28-39, Dec. 1966.

56. A. E. Nielsen, "Kinetics of Precipitation" (Macmillan Co., New York, 1964).

57. James, Pond & Clark, Inc., Pasadena, Calif., Forms 3S-2391R 7-65 and 3S-2421 3-65.

58. Eastern Industries, Hamden, Conn.

59. E. M. Cohn, personal communication.

Fig. 1. Solubilities of O_2 and H_2 in aqueous KOH solutions:

a. O_2 at 15-100 °C

b. H_2 at 21-75 °C

c. H_2 at 170-200 °C

FIG. 1a.

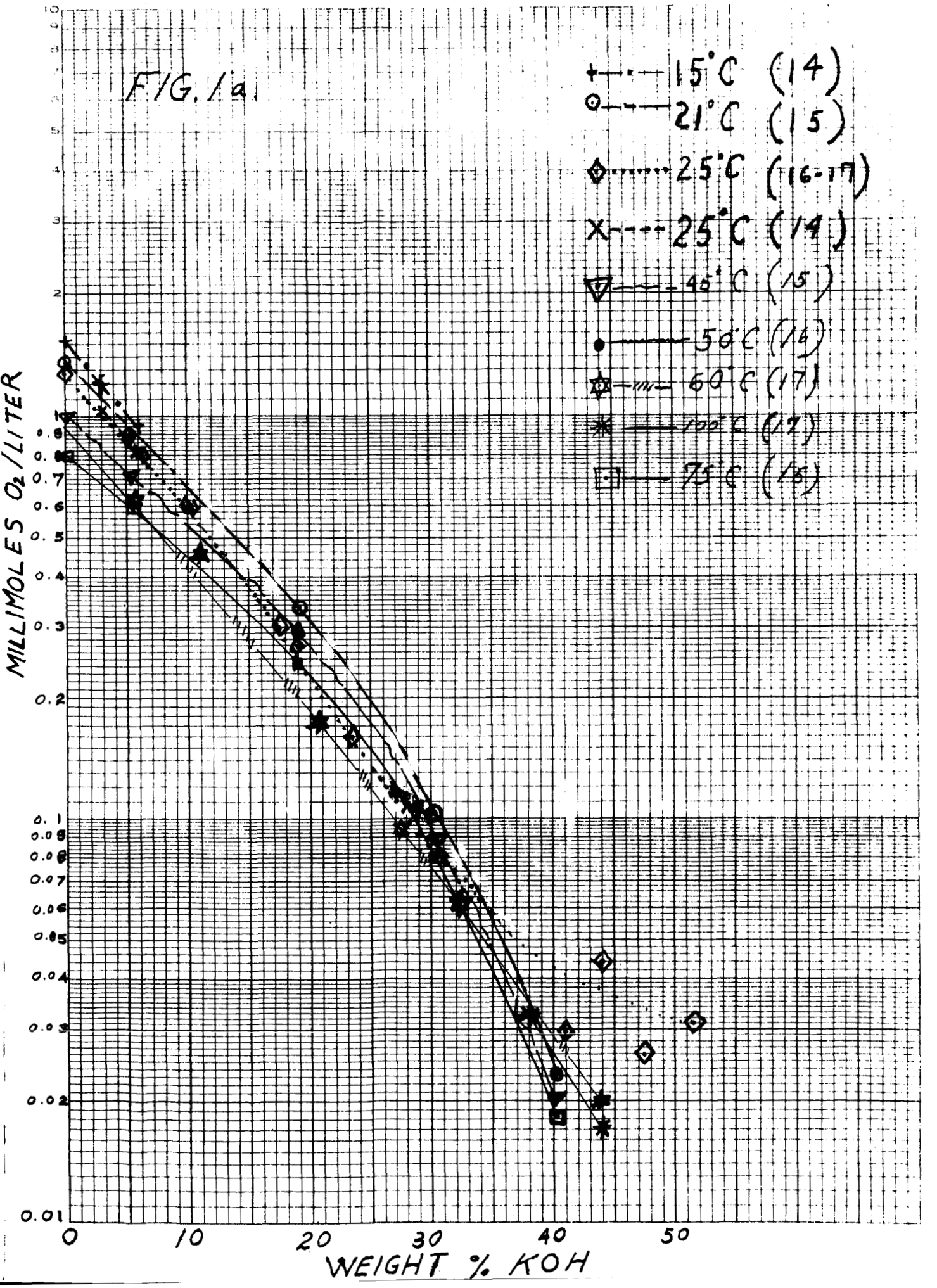
15°C (14)
21°C (15)
25°C (16-17)
25°C (14)
45°C (15)
50°C (14)
60°C (17)
100°C (17)
75°C (15)
MILLIMOLES O2/LITER
WEIGHT % KOH
0
10
20
30
40
50
0.01
0.02
0.03
0.04
0.05
0.06
0.07
0.08
0.09
0.1
0.2
0.3
0.4
0.5
0.6
0.7
0.8
0.9
1
2
3
4
5
6
7
8
9
10

FIG. 1b

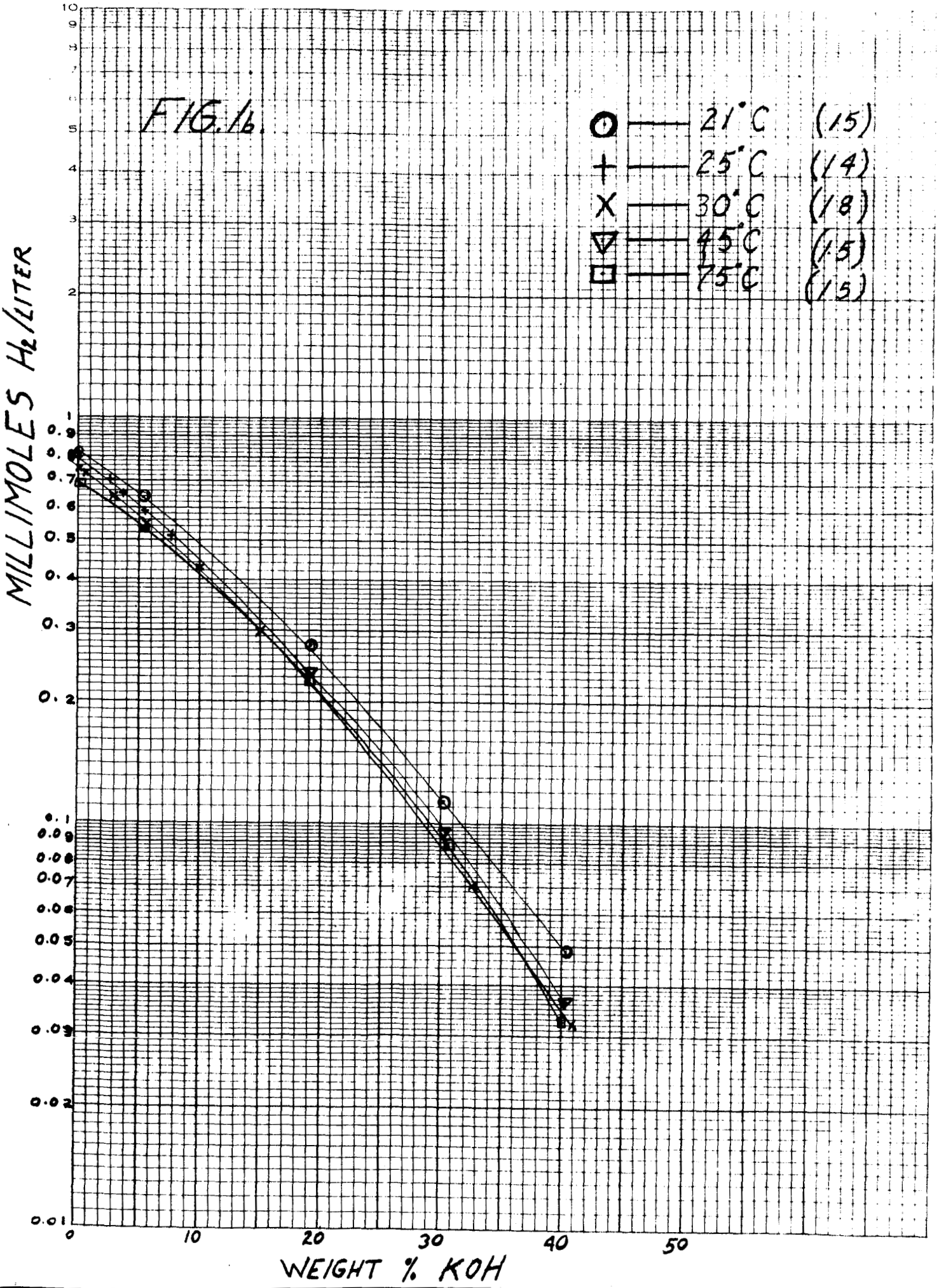
MILLIMOLES H2/LITER
WEIGHT % KOH
21° C (15)
25° C (14)
30° C (18)
45° C (15)
75° C (15)

FIG. 1c.

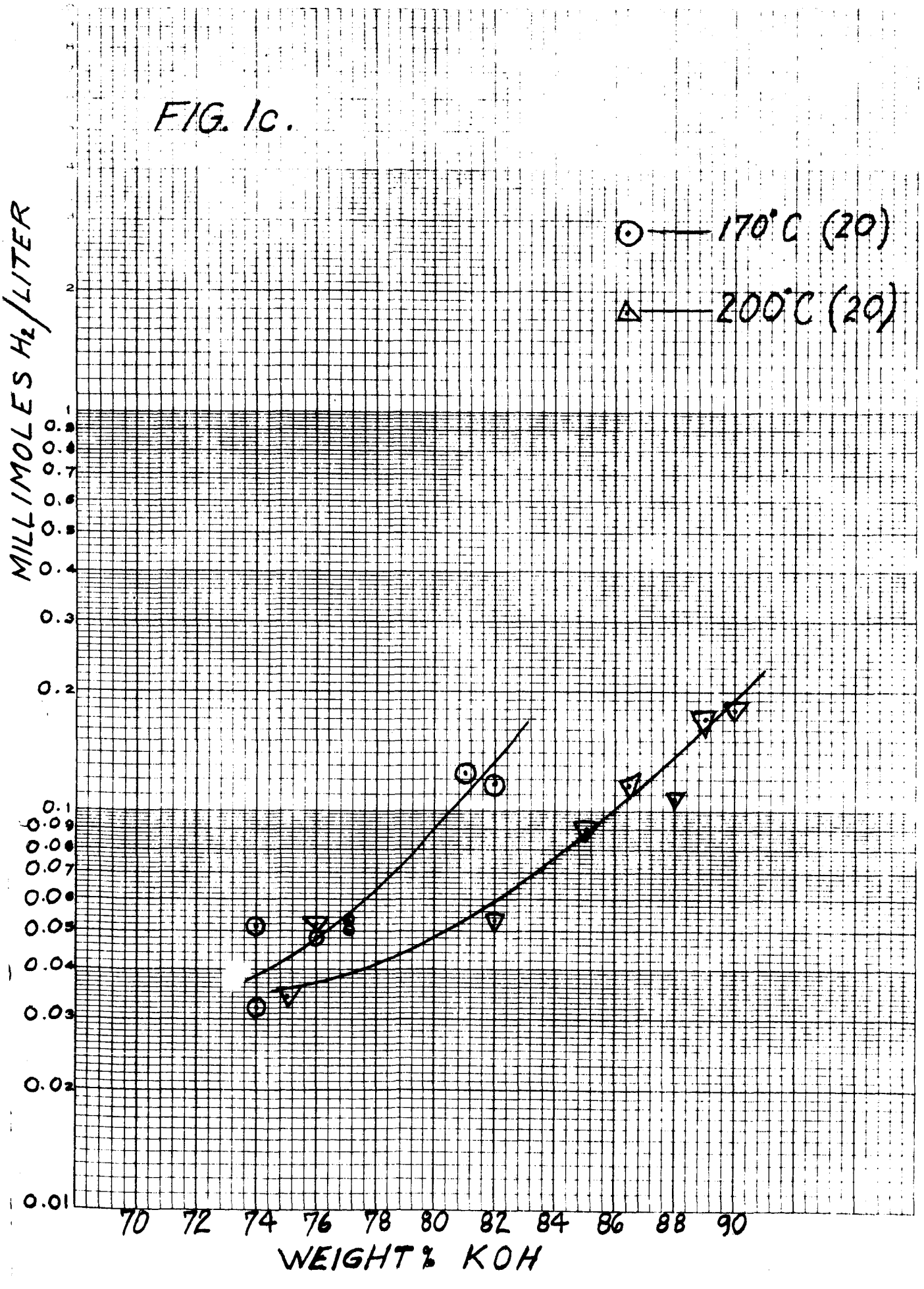
170°C (20)
200°C (20)
MILLIMOLES H2/LITER
2
1
0.9
0.8
0.7
0.6
0.5
0.4
0.3
0.2
0.1
0.09
0.08
0.07
0.06
0.05
0.04
0.03
0.02
0.01
70
72
74
76
78
80
82
84
86
88
90
WEIGHT % KOH

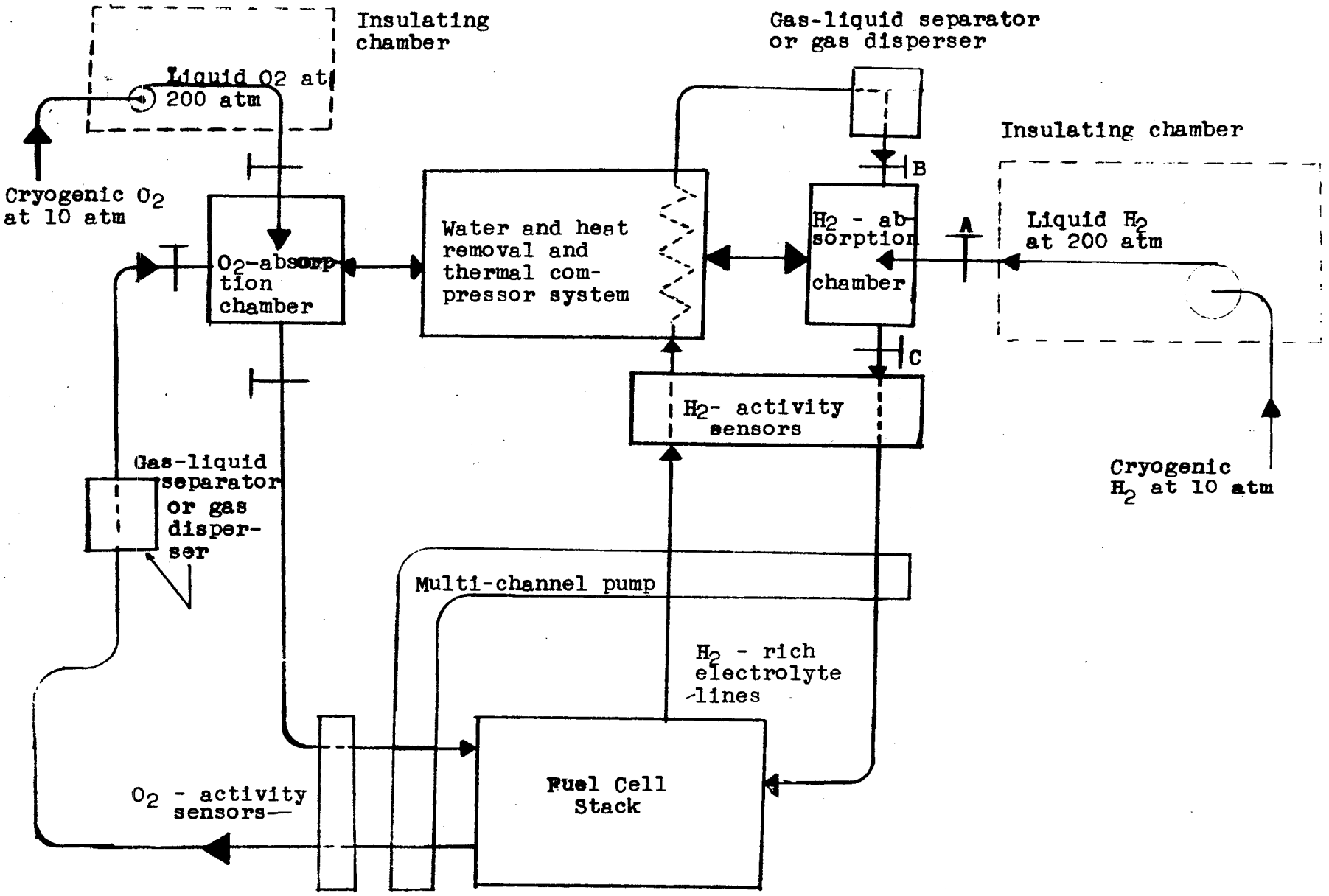

Fig. 2. Electrolyte circulation and saturation system

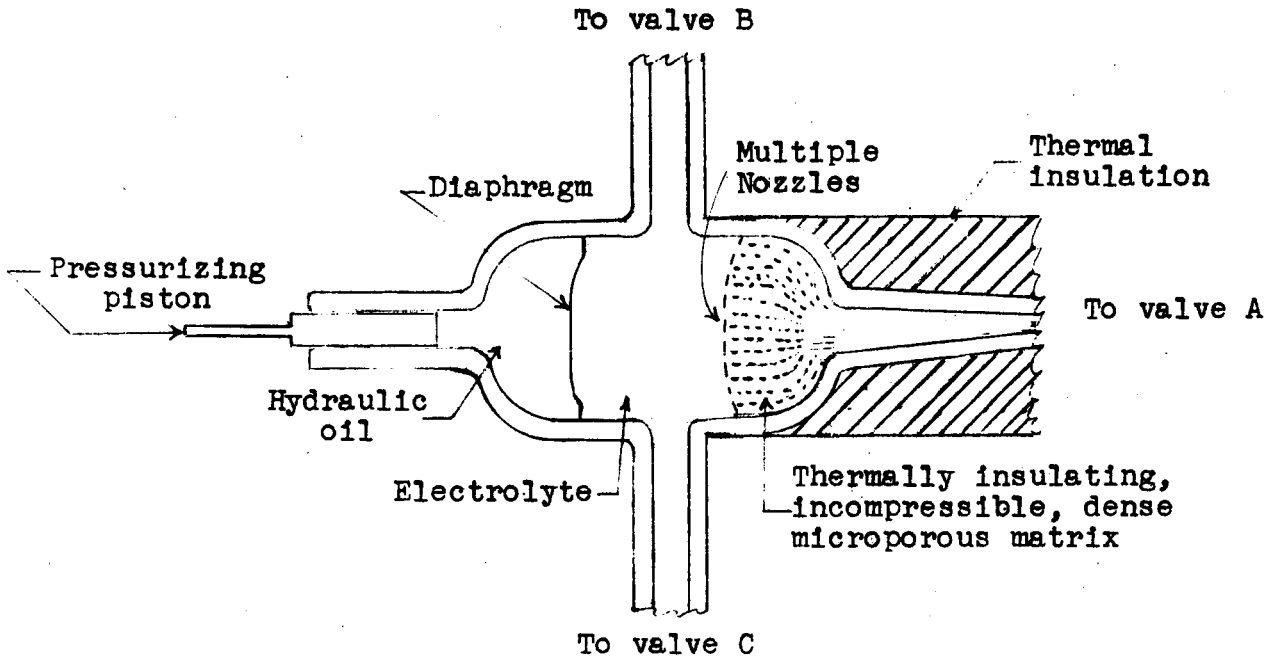

Fig. 3. Saturation chamber

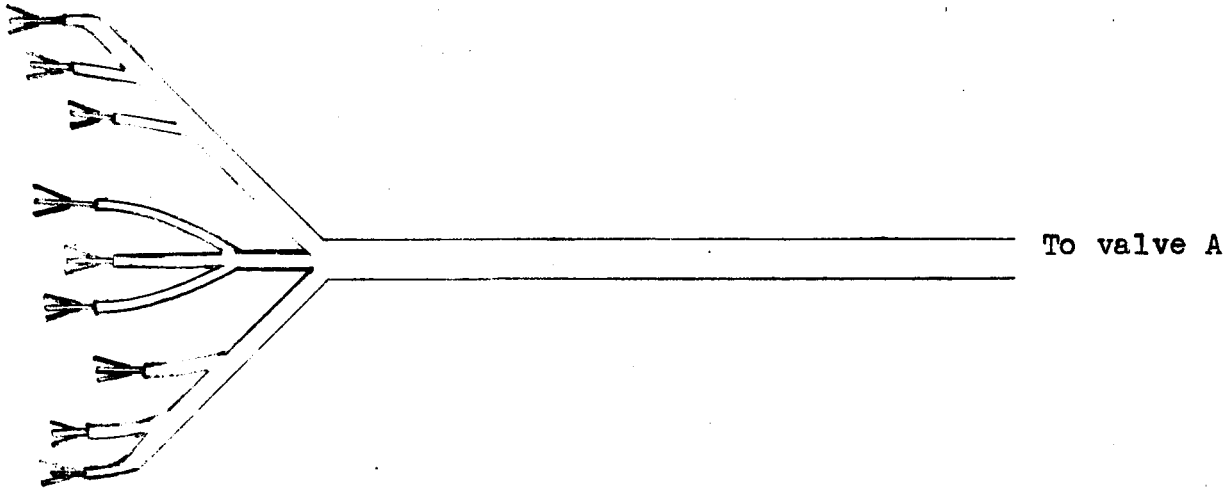

Fig. 4. Multiple nozzle arrangement

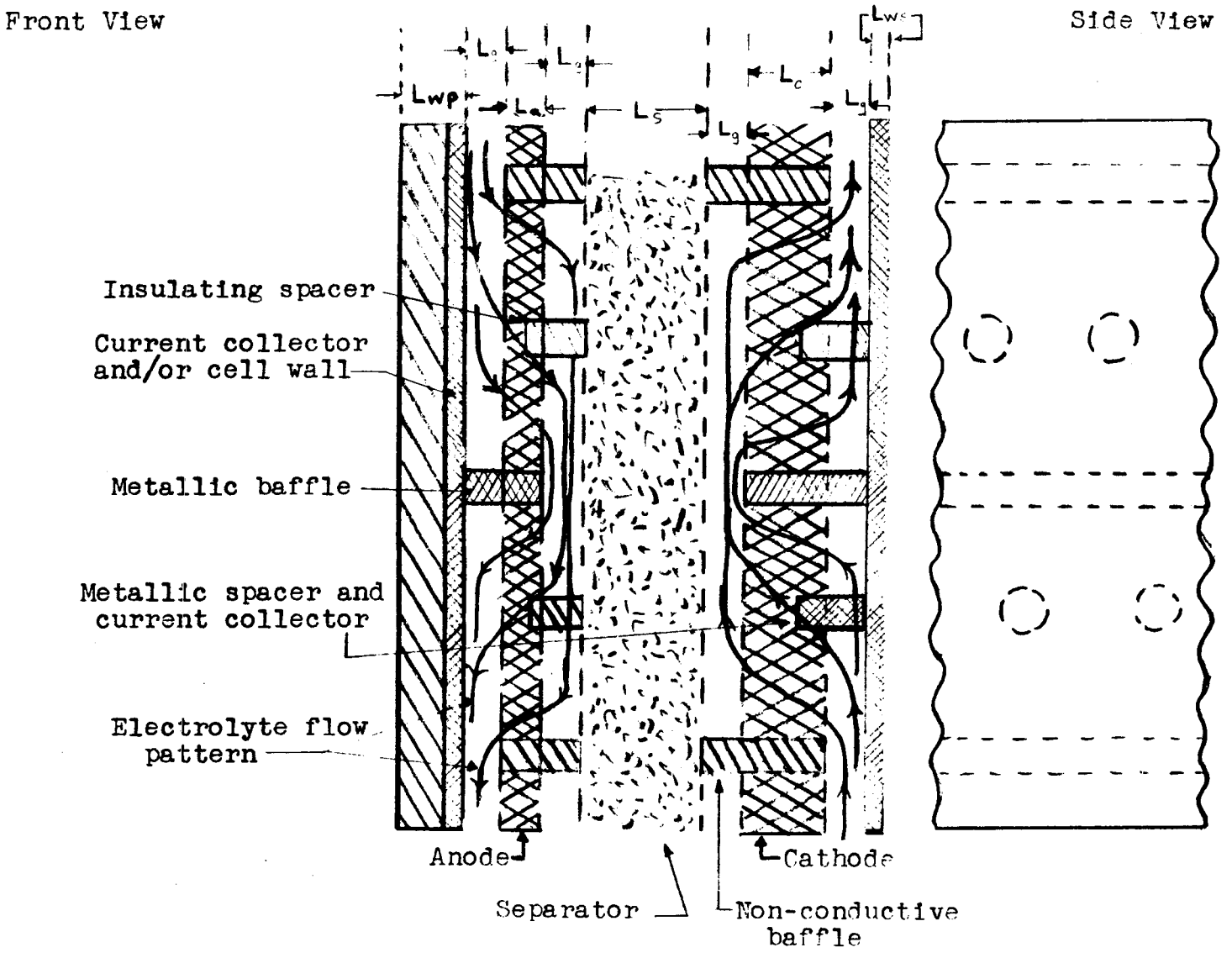

Fig. 5. Single cell configuration. Schematic - not to scale. Horizontal dimensions enlarged by a factor of at least 50.

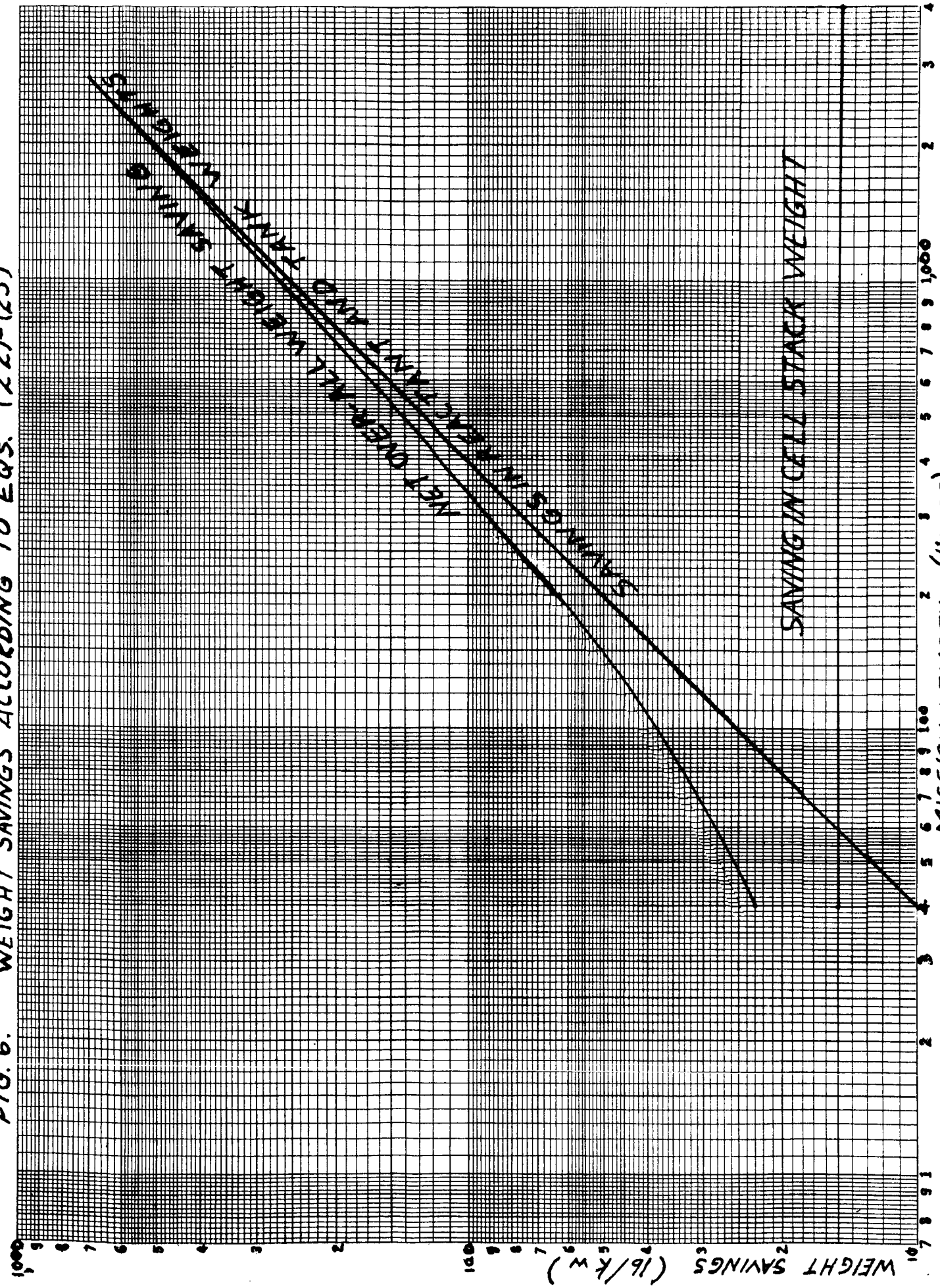

FIG. 6. WEIGHT SAVINGS ACCORDING TO EQS. (22)-(25)